NAVAL POSTGRADUATE SCHOOL

MONTEREY, CALIFORNIA

THESIS

INCREASING UAV ENDURANCE THROUGH INTEGRATING PVDF-BNNT PIEZOELECTRIC ENERGY HARVESTERS ONTO THE AIRFRAME

by

Anna C. Sewall

June 2023

Thesis Advisor: Troy Ansell
Second Reader: Anthony J. Gannon

Approved for public release. Distribution is unlimited.

THIS PAGE INTENTIONALLY LEFT BLANK

REPORT DOCUMENTATION PAGE	*Form Approved OMB No. 0704-0188*

1. AGENCY USE ONLY *(Leave blank)*	**2. REPORT DATE** June 2023	**3. REPORT TYPE AND DATES COVERED** Master's thesis

4. TITLE AND SUBTITLE
INCREASING UAV ENDURANCE THROUGH INTEGRATING PVDF-BNNT PIEZOELECTRIC ENERGY HARVESTERS ONTO THE AIRFRAME

5. FUNDING NUMBERS

6. AUTHOR(S) Anna C. Sewall

7. PERFORMING ORGANIZATION NAME(S) AND ADDRESS(ES)
Naval Postgraduate School
Monterey, CA 93943-5000

8. PERFORMING ORGANIZATION REPORT NUMBER

9. SPONSORING / MONITORING AGENCY NAME(S) AND ADDRESS(ES)
N/A

10. SPONSORING / MONITORING AGENCY REPORT NUMBER

11. SUPPLEMENTARY NOTES The views expressed in this thesis are those of the author and do not reflect the official policy or position of the Department of Defense or the U.S. Government.

12a. DISTRIBUTION / AVAILABILITY STATEMENT
Approved for public release. Distribution is unlimited.

12b. DISTRIBUTION CODE
A

13. ABSTRACT (maximum 200 words)

With the increasing demand for unmanned aerial vehicles (UAVs) for military operations, it is of interest to the Navy to increase these drones' flying endurance. Current solar-powered and battery-powered UAVs have limited capabilities and technical challenges, such as weather dependency and long charging times. This project explored the possibility of using piezoelectric materials to extend the flying time of UAVs. Polymeric piezoelectric energy harvesters were both printed using stereolithography and cast in a mold. These harvesters were then tested for piezoelectric activity. Piezoelectricity was not observed despite the fabrication of flexible polymers. A problem with the printed polymers was sample inhomogeneity and low volume for piezoelectric activity. For the molded samples, saturation polarization was likely not achieved during poling. Further testing of the fabrication technique is required.

14. SUBJECT TERMS
piezoelectric composite, energy harvester, unmanned aerial vehicle, UAV

15. NUMBER OF PAGES
85

16. PRICE CODE

17. SECURITY CLASSIFICATION OF REPORT	**18. SECURITY CLASSIFICATION OF THIS PAGE**	**19. SECURITY CLASSIFICATION OF ABSTRACT**	**20. LIMITATION OF ABSTRACT**
Unclassified	Unclassified	Unclassified	UU

NSN 7540-01-280-5500

Standard Form 298 (Rev. 2-89)
Prescribed by ANSI Std. 239-18

THIS PAGE INTENTIONALLY LEFT BLANK

Approved for public release. Distribution is unlimited.

INCREASING UAV ENDURANCE THROUGH INTEGRATING PVDF-BNNT PIEZOELECTRIC ENERGY HARVESTERS ONTO THE AIRFRAME

Anna C. Sewall
Ensign, United States Navy
BS, United States Naval Academy, 2022

Submitted in partial fulfillment of the
requirements for the degree of

MASTER OF SCIENCE IN ASTRONAUTICAL ENGINEERING

from the

NAVAL POSTGRADUATE SCHOOL
June 2023

Approved by: Troy Ansell
Advisor

Anthony J. Gannon
Second Reader

Brian S. Bingham
Chair, Department of Mechanical and Aerospace Engineering

THIS PAGE INTENTIONALLY LEFT BLANK

ABSTRACT

With the increasing demand for unmanned aerial vehicles (UAVs) for military operations, it is of interest to the Navy to increase these drones' flying endurance. Current solar-powered and battery-powered UAVs have limited capabilities and technical challenges, such as weather dependency and long charging times. This project explored the possibility of using piezoelectric materials to extend the flying time of UAVs. Polymeric piezoelectric energy harvesters were both printed using stereolithography and cast in a mold. These harvesters were then tested for piezoelectric activity. Piezoelectricity was not observed despite the fabrication of flexible polymers. A problem with the printed polymers was sample inhomogeneity and low volume for piezoelectric activity. For the molded samples, saturation polarization was likely not achieved during poling. Further testing of the fabrication technique is required.

THIS PAGE INTENTIONALLY LEFT BLANK

TABLE OF CONTENTS

LIST OF FIGURES

THIS PAGE INTENTIONALLY LEFT BLANK

LIST OF TABLES

THIS PAGE INTENTIONALLY LEFT BLANK

LIST OF ACRONYMS AND ABBREVIATIONS

3D	three-dimensional
Ag	silver
AM	additive manufacturing
Ar	argon
BNNT	boron nitride nanotube
CNT	carbon nanotube
d_{ik}	piezoelectric charge constants
DMF	dimethylformamide
DMSO	dimethyl sulfoxide
DNF	did not finish
FFF	fused filament fabrication
HV	high voltage
IPA	isopropyl alcohol
LiPo	lithium-ion polymer
Pd	palladium
PR	photopolymer resin
Pt	platinum
PVDF	polyvinylidene fluoride
RPM	revolutions per minute
STL	stereolithography
TrFE	trifluoroethylene
UAV	unmanned aerial vehicle
Wt%	weight percent

THIS PAGE INTENTIONALLY LEFT BLANK

ACKNOWLEDGMENTS

I would firstly like to thank the plethora of tutors at the Graduate Writing Center for their help with correcting my writing. To list the name of each tutor to whom I sent drafts would require another subsection within this thesis, so I will avoid one-by-one acknowledgment. However, I felt it necessary to recognize how grateful I am to every one of them for taking the time to read about a topic that is not the most exciting for someone not in the engineering community (or even someone within it, I suppose).

I would also like to thank Professor Anthony Gannon for being my second reader and for courageously allowing a one-year Bowman Scholar student access to an exclusive drone. Even though he might have initially agreed to let me operate the UAV because I am listed as a Shoemaker Scholar in Python and he thought I was going to flight school upon graduation, I'm sure that in the future the submarine community will be grateful for my ability to steer an expensive machine.

I also must throw in a shoutout here to my roommates, Brinley and Katie, for their help on this graduate school journey. Although being one of the very few Ensigns in a sea of higher-ranking officers at NPS could be intimidating at times, nothing in this past year was as terrifying as texting our landlord that we had broken something else in his house. I am thankful that my fellow "Ladies of Destruction" were by my side for this adventure.

Last, but certainly not least, I would like to thank my advisor, Dr. Troy Ansell, for allowing me to be the first student to conduct research on his idea of integrating energy harvesters onto the airframe of a UAV. As a mechanical engineering undergraduate student who had the random urge to switch my major to astronautical engineering in graduate school, I clearly wanted to remain in the field I had studied for four years previously when it came to my thesis, and Dr. Ansell allowed that. Through my numerous last-minute meeting cancellations, ridiculously long emails detailing my tiniest findings, and constant requesting of "Hey Sir, can you check out my latest draft?" Dr. Ansell was truly the best advisor I could have imagined, and I am so appreciative that he let me join his team.

THIS PAGE INTENTIONALLY LEFT BLANK

I. INTRODUCTION

A. MOTIVATION

With the increasing demand for unmanned aerial vehicles (UAVs) to perform military operations, it is of interest to the Navy to increase their flying endurance. Current solar-powered and battery-powered UAVs have limited capabilities and technical challenges. Some of these issues include weather dependency and long charging times. This project explores the possibility of using piezoelectric materials to extend the flying time of UAVs: more specifically, attaching three-dimensional (3D) printed piezoelectric energy harvesters onto the airframe to assist with increasing the UAVs' endurance.

To date, there has been limited research on extending the flying endurance of UAVs by attaching piezoelectric energy harvesters to their airframes. This thesis aims to investigate the feasibility of attaching energy harvesters to a UAV's airframe that are lightweight, provide measurable charge, and increase battery lifeline, such as polyvinylidene fluoride (PVDF) polymers. To increase the energy-harvesting ability of PVDF, composites with a filler of boron nitride nanotubes (BNNTs) will be fabricated.

B. OBJECTIVES

The overall objective of this thesis is to extend the endurance of UAVs by connecting a piezoelectric energy harvester to the battery. Ideally, the piezoelectric element will be able to compensate for some of the load on the battery by harnessing part of the vibrational energy within the system. Using stereolithography, composites of PVDF and BNNTs will be printed. Should printing fail, the composites will be cast using a mold. The fabricated harvesters will undergo poling and materials and mechanical characterization. The actual testing of harvester performance on a UAV will be performed after piezoelectric properties are confirmed.

C. THESIS OUTLINE

Chapter I gave a brief introduction to the thesis, while a literature review is found in Chapter II. The project's experimental procedures are discussed in Chapter III, and

Chapter IV includes the experimental results and a discussion of them. Conclusions and recommendations for future work are discussed in Chapter V.

II. LITERATURE REVIEW

A. INTRODUCTION

The following sections showcase a literature review, which introduces some current issues with the flying endurance of Unmanned Aerial Vehicles (UAVs). This literature review also provides an in-depth review of the science behind the fabrication methods of the energy harvesters that will be made and tested to fix these UAV flying-time shortcomings.

B. CURRENT ENDURANCE ISSUES OF UAVS

UAVs, commonly referred to as drones, are flying devices with no human passengers. They are typically remote controlled or have computers onboard that execute a predetermined mission set [1]. In the Navy, autonomous vehicles provide safer operations such as object detection and tracking, security, and hazardous area surveillance since no human is onboard [2]. Additionally, UAVs can be useful in the case of a manpower shortage. In the civilian sector, traffic observation, navigation, post-disaster operations, and healthcare are just a few of the many UAV applications [2]. UAVs are deployed in numerous mission-sets that correlate to overall enhanced operations, which includes saving human lives. One of the ways to improve performance during these missions is to extend the flying endurance of the drones, because a longer flying time would allow for an extended period to execute any given assignment. The endurance is ultimately tied to the performance of onboard batteries, batteries with solar cells, or some other onboard power source.

Current solar-powered and battery-powered UAVs have limited capabilities and technical challenges, including weather dependency, limited battery capacity, and long charging times. The weight of the drone and its batteries can limit the drone to shorter missions and/or limited navigation [2]. The limited battery-power within UAVs is arguably the most significant issue. This issue limits flight duration significantly and therefore UAVs are unable to complete certain objectives in emerging missions [3]. This limitation is mainly due to the fixed lithium-ion polymer (LiPo) battery, which powers an estimated

most drones [3]. Numerous studies have been conducted to try to overcome the battery restriction, including "UAV or battery hot-swapping, battery capacity increase, UAV placement or path optimization," and more, all of which have failed to deliver substantial flying time increases [3].

To overcome the flying restrictions imposed by the limitations of the battery issues, this thesis will focus on fabricating piezoelectric polymer-composite energy harvesters and attaching them onto the airframe of a UAV. Once attached, the composite could remove some of the electrical load on the battery by harvesting the vibrational energy. Removing part of the load on the battery would lengthen the flying time of the UAV.

C. ADDITIVE MANUFACTURING

Additive manufacturing (AM) is the construction of a three-dimensional object from a digital model. The additive process for all AM productions consists of solid model generation, file generation, model slicing, and then physical printing of the model using either resin or filament [4]. This project utilized resin, specifically FormLab's clear photopolymer resin (PR), for the physical printing of the piezoelectric element. In addition to the different AM print materials, there are many types of AM methods, including stereolithography (STL), fused filament fabrication (FFF), powder bed methods, and directed energy methods. The two AM approaches considered for printing the piezoelectric energy-harvester for this thesis were FFF and STL.

FFF, also referred to as fused deposition modeling, is a process whereby the melted filament is extruded through a heated nozzle one layer at a time in a fine stream [4]. The layers are fused together and solidified onto a build platform and the final piece can be taken off the platform with minimal post-processing necessary [5]. This method is one of the most commonly used processes because of its rapid printing, simple operation, and low cost [6]. The advantages of using the FFF printing method in relation to the printing of piezoelectric polymers includes the lack of harsh chemicals when printing/post-processing and the compact nature of the equipment itself [6]. A major disadvantage is that with FFF, most of the published studies focus on the printing of pure polymer materials [6]. This is a

shortcoming as it is unknown whether FFF can be used to print polymer composites. Additionally, FFF parts have been found to have poor tensile strength, a mediocre surface finish, and poor interlayer adhesion since each layer of the polymer solidifies as it is laid on the build plate [7]. Therefore, this study focuses on printing polymer nanocomposite energy harvesters via the STL approach.

Like FFF, STL is commonly used when 3D printing polymers. An analysis of STL's pros and cons was conducted before its selection as the process used to print the energy harvesters. STL is a method of AM wherein a laser beam, typically at Ultraviolet wavelength, is moved over a liquid resin following a digital model just like in FFF [4]. The liquid resin contains a photopolymer, which polymerizes upon exposure to light with a wavelength specific to the photopolymer: the resin hardens in a relatively short time period due to the induced polymerization of the photopolymer [4]. This process is computer-controlled and builds up the desired object layer by layer, hardening the liquid resin when it comes in contact with the laser [4].

Many experts in the field of AM prefer STL printing because it provides high-quality finishes as well as an intense level of detail on printed pieces [4]. STL printers can fabricate various materials with different properties in a small and compact workspace [4]. Additionally, STL is able to uniformly cross-link the polymer chains, allowing superior mechanical properties of its prints as compared to FFF [7]. Some disadvantages of STL printing include the use of unsafe chemicals, curing of the part post-printing, and the need for supports on most prints [4]. However, because the printed pieces will be small and relatively simple in design, STL was selected for printing.

D. PIEZOELECTRICITY AND ENERGY HARVESTING

Piezoelectricity is the property of certain materials whereby an electric charge is generated when a mechanical stress or vibration is applied [8]. This phenomenon is called the direct piezoelectric effect and it is harnessed for use in accelerometers, surface acoustic wave sensors, and any piezoelectric sensor [8]. Piezoelectric materials must have a crystal (or molecular) structure that is non-centrosymmetric to convert the mechanical energy to

electrical energy [9]. To be non-centrosymmetric, the elements in the unit cell, or monomer in the case of piezoelectric polymers, must be arranged such that the charge balance is non-zero (i.e., a polarization exists). Energy harvesting is the ability to generate power from external sources such as mechanical vibrations and use that power to provide energy to an array of devices, or in this case, a UAV [9].

Piezoelectric materials are of interest when considering nanoscale energy harvesters because the generated electric fields from the piezoelectric polymers can be controlled and utilized in such devices [10]. Piezoelectric energy harvesting is desirable over other types of energy harvesting because "it does not require a separate voltage source, magnetic field, or contact with another material" as do other mechanisms such as electromagnetic or electrostatic harvesting [9]. Because of its solidarity, reliability, and durability, piezoelectric energy harvesting provides more promising qualities to use in systems such as wireless electronics, including UAVs.

E. POLYVINYLIDENE FLUORIDE POLYMERS AND COMPOSITES

Lower mass piezoelectric polymers would be better suited for UAV based energy-harvesting. Among the known piezoelectric polymers, polyvinylidene fluoride (PVDF) is the most commonly used: this includes applications in energy harvesting [11]. PVDF is "inexpensive, environmentally friendly, lightweight, conformable, and has a fast response time," making it a leading contender for various applications [11]. More importantly, PVDF has the highest piezoelectric coefficient among polymers, reaching -30 pC/N in some studies [12]. Because of the numerous benefits that PVDF offers over other piezoelectric polymers, it was chosen as the material that would be tested to increase the flying endurance of the UAV.

An important concept concerning PVDF fabrication is its associated alpha (α) and beta (β) phases. The α-phase of PVDF is never piezoelectric, while the β-phase, PVDF's most electroactive polymorph, is piezoelectric [9]. The crystal structures of both polymorphs can be seen in Figure 1.

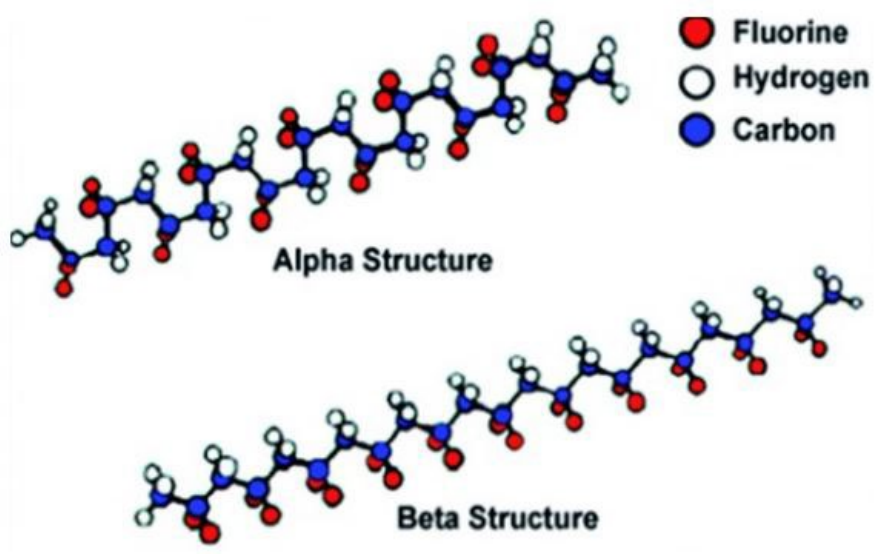

Figure 1. The chain conformation of the alpha and beta crystalline phases of PVDF. Adapted from [13].

Looking at one monomer of α-PVDF in Figure 2a, pairs of hydrogen atoms occupy positions directly across the transverse axis from each other [13]. The same is true for pairs of fluorine atoms. The separation of the oppositely charged pairs leads to a polarization. However, since there is also a polarization of equal magnitude in the opposite direction, the polarization is cancelled. Conversely, for the β-PVDF monomer shown in Figure 2b, the opposing positions of the hydrogen atoms, each with a positive charge, and the negatively charged fluorine atoms lead to a non-zero polarization [13].

It is difficult to force pure PVDF into the β-phase. The β-phase is the most sought after phase due to its crystalline region, which contains a "planar zigzag conformation," that provides the largest dipole moment of all PVDF crystalline phases [13]. One method of getting pure PVDF into the desired phase is stretching it to rearrange the chain conformation [5]. Achieving this transition from α-phase to β-phase can be a tedious process, however, which is why copolymers and composites are introduced. Copolymers and composites can improve the performance of the pure polymer to ensure formation of the β-phase and harness its dipole moment.

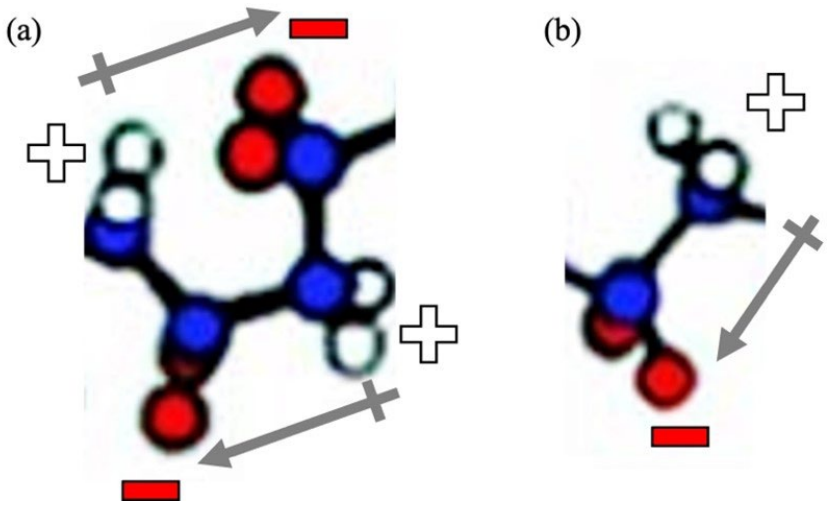

Figure 2. Individual monomers of α-PVDF (a) and β-PVDF (b). Adapted from [13].

A commonly used copolymer of PVDF is trifluoroethylene (TrFE) because it forces PVDF into the β-phase [14]. The PDVF-TrFE copolymer will be used in this energy-harvesting experiment because it exhibits advantages for microelectronic applications, as studies have revealed that it "shows much higher crystallinity and a larger piezoelectric response" [15]. The PDVF-TrFE composite can come in many different ratios; for this research, a 70% PVDF-30% TrFE composite was used. For the remainder of this thesis, the copolymer PVDF-TrFE will be referred to as just PVDF. If PVDF without the copolymer is mentioned, it will be referred to as "pure" PVDF.

F. BORON NITRIDE NANOTUBES

1. Intrinsic Properties

Although PVDF is a strong candidate for piezoelectric polymers, some physical properties of the material are not ideal; therefore, nanofillers will be added. Nanomaterials are particles with dimensions smaller than 100 nanometers that can be added to other substances to change their composition and improve their physical properties [16]. Boron nitride nanotubes (BNNTs) have been a nanostructure of interest in materials science since their discovery and synthesis in 1995 and because of their impressive intrinsic properties [17]. For example, BNNTs could be beneficial in operating environments due to their

higher thermal stability in high-temperature environments (as compared to the more well-known and studied carbon nanotubes (CNTs)) and oxidation resistance behavior. Additionally, BNNTs exhibit neutron radiation shielding capability, high strength-to-weight ratio, and exceptional piezoelectric and mechanical properties [18]. These benefits relate to important mission-sets that UAVs may need to endure in the Navy; therefore, BNNTs were added to the PVDF resin for this research.

2. BNNTs versus CNTs

It is important to acknowledge the main contender for BNNTs, as CNTs are another impressive nanofiller with several applications and properties that are similar to BNNTs and also potentially useful for UAV research. CNTs are used in similar projects as BNNTs, with good mechanical strength and high thermal conductivity; however, they are not piezoelectric like BNNTs [16]. Additionally, BNNTs have been proven to work more effectively in polymers, as studies have shown that BNNTs form better binding interfaces with polymers than CNTs do [16].

Another property of interest to compare between BNNTs and CNTs is electrical insulation: BNNTs are electrically insulated while CNTs are conductive [16]. Additionally, BNNTs can be polarized and have the ability to shield neutron radiation [19]. Due to these benefits, and the fact that CNTs are not piezoelectric, BNNTs are a superior option for composites where high thermal properties, strong mechanical properties, or electrical insulation are desired, such as environments where UAVs may need to operate.

3. BNNT Applications

Due to their stability in high-temperature environments, BNNTs could "be integrated with various polymers to create a new class of thermal conductive BNNT-polymer composite" for several civilian uses, such as packaging materials [17]. Even more impressive, BNNTs have recently been studied in the fields of water-purification and oil-filtering, as well as biologically in the form of a drug carrier in patients [17]. For military applications, operational environments could be made safer due to BNNTs' ability to remain stable at high-temperature environments. Also, the high cross-section for neutron absorption allows equipment guarded by this nanomaterial to operate in hot and radiative

surroundings [18]. Neutron absorption could be particularly of interest in space exploration. Interaction of neutrons and cosmic radiation with matter in space has been known to cause malfunctions and permanent damage to gear and astronauts [17]. BNNTs could be an exceptional nanomaterial in shielding equipment for both the space environment and the air environments in military operations, which is why it will be tested in this research.

G. DIMETHYL SULFOXIDE

Many PVDF/PR mixing projects often utilize solvents, or liquids that dissolve solid material into a solution, to uniformly disperse the PVDF powder into the resin. The PVDF is often mixed into a heated solvent first, and then the resin is poured into that solution once the powder is completely dissolved. Studies have shown that incorporating a solvent allows the PVDF powder to blend more homogeneously with the PR, avoiding agglomerates of powder being left in the mixture [7]. The solvent typically used to dissolve PVDF is Dimethylformamide (DMF). DMF, however, is toxic. An alternative solvent is Dimethyl sulfoxide (DMSO), which is relatively non-toxic with one caveat: DMSO can easily penetrate human skin. Therefore, if DMSO contains any solute, it can potentially transport that solute into the human body.

When choosing between solvents, several parameters could have been considered, one of those being the dielectric constant of the material. Solvents with a higher dielectric constant, which will be discussed more, are able to store more energy [20]. Larger dielectric constant materials also have better electric susceptibility, or ability to be polarized, both of which are principal factors in this thesis [20]. Between the two considered solvents, DMF has a lower dielectric constant of 36, while DMSO has a higher dielectric constant of 47, a significant difference [20]. Not only is DMSO a higher-performing solvent for the applications it was needed for, but it is also less toxic than DMF [21]. Because DMSO is safer to handle and is more easily polarized, it was chosen above its similar counterpart solvent, DMF.

Surface images of different mixtures of PVDF and PR with and within solvents are shown in Figure 3. Figures 3(a) and 3(b) show several white clumps, proving that without

solvent, a significant amount of PVDF particles can collect within the PR rather than providing a smooth mixture. Figure 3(c) shows the pure PR for comparison purposes to display how Figures 3(d) and 3(e) also have hardly any white clumps of PVDF left in them after using solvent. It is also important to note that the white particles in Figure 3(c), the pure PR, are "debris or contaminates" rather than agglomerates of powder [7].

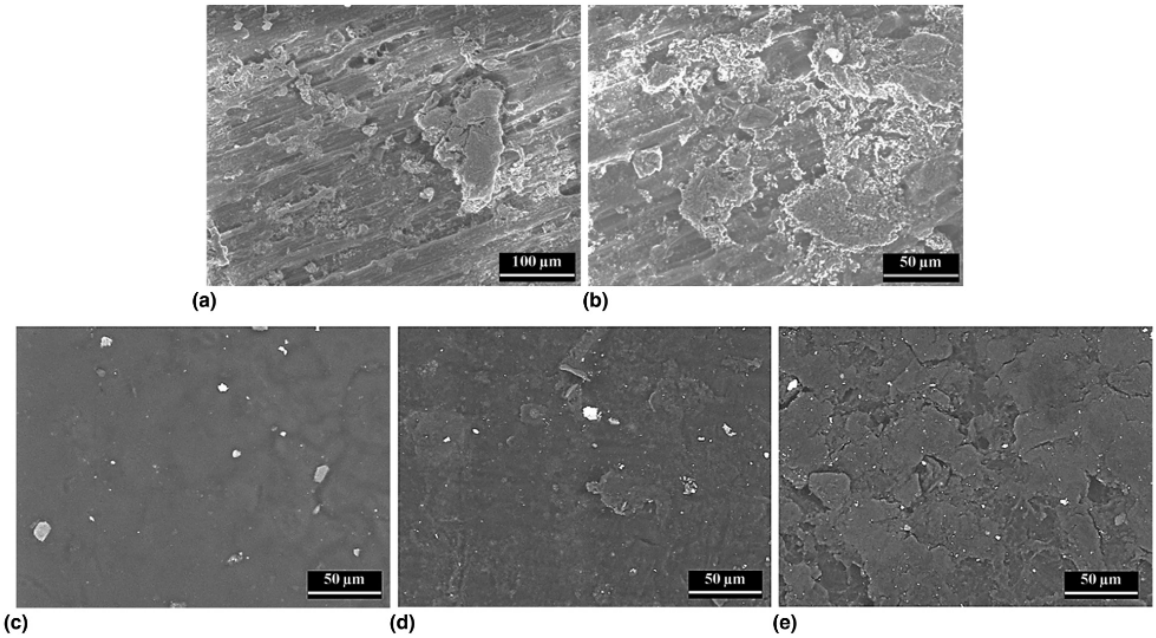

Figure 3. Surface images of 3D-printed PVDF/PR blends with and without a solvent: 5 wt% PVDF/PR without solvent treatment (a and b); pure PR (c), 2 wt% PVDF/PR with solvent treatment (d); and 5 wt% PVDF/PR blend with solvent treatment (e). Source: [7].

H. METAL SURFACE SPUTTER COATING

Because piezoelectric materials are insulators, these materials must have conductive electrodes to generate charge and carry a current away, similar to a capacitor. One of the common approaches to metallizing piezoelectric materials is by coating the surface through sputter coating, a method of applying a thin coat of metal onto an object. Also referred to as sputtering, this approach's main goal is to modify the functionality of the piece that is coated, and improve surface properties such as hardness, roughness,

corrosion resistance, and more [22]. Sputter coating on a microscopic level is "the physical ejection of atoms from a surface because of the bombardment of the surface by energetic particles" in the presence of an inert gas [23]. Here, the printed piezoelectric squares were sputter coated with an 80/20 platinum/palladium (Pt/Pd) oxide coating in order to assist with creating a circuit during the poling process, as well as to improve the piezoelectric element's surface properties.

Sputtering is easy to perform, inexpensive, and very common in engineering applications [22]. Additional benefits of this method include simple and accurate adjustments of the thickness of the layers of metal, and the numerous different coating metals that can be used for the sputtering material [24]. The process of sputter coating regarding its use in this research will be discussed more in Chapter III; however, as previously stated, Pt/Pd was the noble metal, or corrosion resistant metal, used in this research due to its light weight. Argon (Ar) gas was the inert gas used to fill the chamber where the sputtering takes place.

I. CONTACT POLING

The application of a high electric field to certain materials results in dipole alignment within the material; one way of conducting this alignment is called contact poling, and it was performed on the metal-coated piezoelectric elements in this research [25]. The contact poling process is a means of electrically aligning diploes within a material so that they exhibit a polarization. For example, because poling allows for the orientation of dipoles along the field direction by applying an external electric field, it initiates piezoelectricity in certain materials by switching the "polar axis of crystallites to the symmetry-allowed directions nearest to the applied field," meaning the field aligns the dipoles to make materials electromechanically active [26]. Contact poling requires "physical contact of the live electrode with the sample electrode" along with the large electric field to correctly pole the piece [26]. The tested samples are coated with both a top and bottom electrode for this technique because it creates a capacitor to hold charge [26]. The samples are then placed in silicon oil and heated while the voltage is applied and the poles aligned, if successful.

The exact poling process regarding this research will be discussed more in Chapter III; however, the dimensions of the piezoelectric pieces play a crucial role in poling. First, the metallized surfaces help to optimize the poling process because charge is spread across the whole surface when covered with metal; therefore, if more surface area is coated, then there is a better chance of successfully poling. Additionally, the electric field that is applied to the piezoelectric element can be expressed as

$$F = \frac{V}{t}, \tag{1}$$

where F is the generated electric field in units of volts per millimeter, V is the voltage applied to the sample in units of volts, and t is the thickness of the sample in units of millimeters. Equation (1) shows that the applied voltage is chosen based on the thickness of the element and the desired electric field, which for PVDF, was chosen to be 5.0 kV/mm. A thinner piece facilitates easier poling; however, a thicker piece handles higher voltages more successfully without damaging the sample. Initial applied voltage was calculated based on the thickness of the piece and a targeted 5.0 kV/mm electric field; however, the voltage was sometimes increased when testing the samples, which will be discussed more in Chapter III.

J. PIEZOELECTRIC CHARGE CONSTANTS

Piezoelectric charge constants (d_{ik}) are anisotropic physical quantities that measure how well a certain material converts mechanical stress into electric charge: this parameter was measured in all of the metal-coated prints for this thesis [27]. This parameter relates the electric charge generated from a material per unit area with an applied force and therefore has units of Coulombs per Newton; however, the measurements are so small that the units are typically expressed on pC/N. [8]. Many variations of measured charge constants are possible, as this parameter allows for varying magnitudes according to the measuring directions and anisotropy in the crystal structures. [27]. The direction of the constants is denoted within the symbol d_{ik}. The two subscripts "i" and "k" are always replaced with numbers that denote the different directions of the measurement, where the "i" is the direction of the electric field and "k" is the direction of mechanical stress [27].

The piezoelectric charge constant that was examined in this thesis was d_{33}. d_{33} applies to a system when the aforementioned mechanical stress is parallel with the polarization axis [8]. It is important to note that with the d_{33} parameter, the force acts on the same surface from which the charge is collected [8]. The d_{33} constant was measured in this research both before and after poling the created samples, which will be discussed more in Chapter III. A successful test would provide an increase in the d_{33} value because that would mean that the piezoelectricity within the piece had improved.

III. EXPERIMENTAL METHODS

A. INTRODUCTION

This chapter covers the fabrication methods of the piezoelectric elements, from the 3D printing methods' initial mixing and production to sputter coating and poling, as well as the molding fabrication method. It also covers problems that occurred along the way and a discussion of how those issues were overcome or how the methods were changed.

B. PRINTING OF PVDF NANOCOMPOSITES

1. Mixing of Resin Solutions

The first step in printing the PVDF composites was to dissolve PVDF-TrFE 70–30 powder (Piezotech™ FC-30, Arkema) in heated DMSO (Thermo-Fisher Scientific). 100 mL of DMSO was poured into a beaker and placed on top of a hotplate. To keep the temperature of the solution consistent, aluminum foil was wrapped over the top of the solvent-filled beaker. A thermometer was inserted through the foil and into the solution and held with a clamp to better monitor the temperature of the liquid. Through trial-and-error, it was found that a hotplate temperature of about 115°C kept the DMSO at the desired mixing temperature of 75°C to 80°C. Once the solvent was heated, the desired number of grams of PVDF was added into 100 mL of DMSO. A magnet mixer spun the mixture at 200 or 400 revolutions per minute (RPM) until the PVDF powder was fully dissolved in the heated solvent. The amount of time for the PVDF to dissolve into the DMSO was noted, and in some cases, small chunks of solid PVDF that did not dissolve within about an hour and a half of mixing were removed from the solution before the PR was added in. The dissolving times varied according to the amount of PVDF, mixer rotation speed, and heat of the hot plate.

After the PVDF powder was dissolved and solids removed, the magnet mixer was left spinning for about 15 minutes to achieve a more thorough mixing. The hotplate was then turned off and the thermometer was removed. The solution was allowed to cool. Once at room temperature, the beaker was replaced on the plate and the magnetic mixer's rotation speed was increased to 600 RPM. The desired amount of clear PR (Clear photoactive resin,

FormLabs), which varied with each mixture, was then added into the PVDF/DMSO solution. After mixing for 20 minutes, the new mixture was funneled into an empty clear resin cartridge for printing. Samples printed with BNNTs had the BNNTs (BNNano) mixed in the as-mixed PVDF-TrFE/DMSO/PR solution and before funneling into the resin cartridge.

2. Resin Printing

Printing of samples was performed in a Form 2 STL printer (FormLabs), as shown in Figure 4. The filled resin cartridge was inserted in the rear of the printer and a resin tank specific to the Clear PR was inserted, as shown by the orange shallow container in Figure 4. A build plate used with all of the printing jobs in this work was inserted at the top. With the correct cartridge and tank inserted, resin was allowed to fill the tank. The orange lid was then lowered to cover the printer.

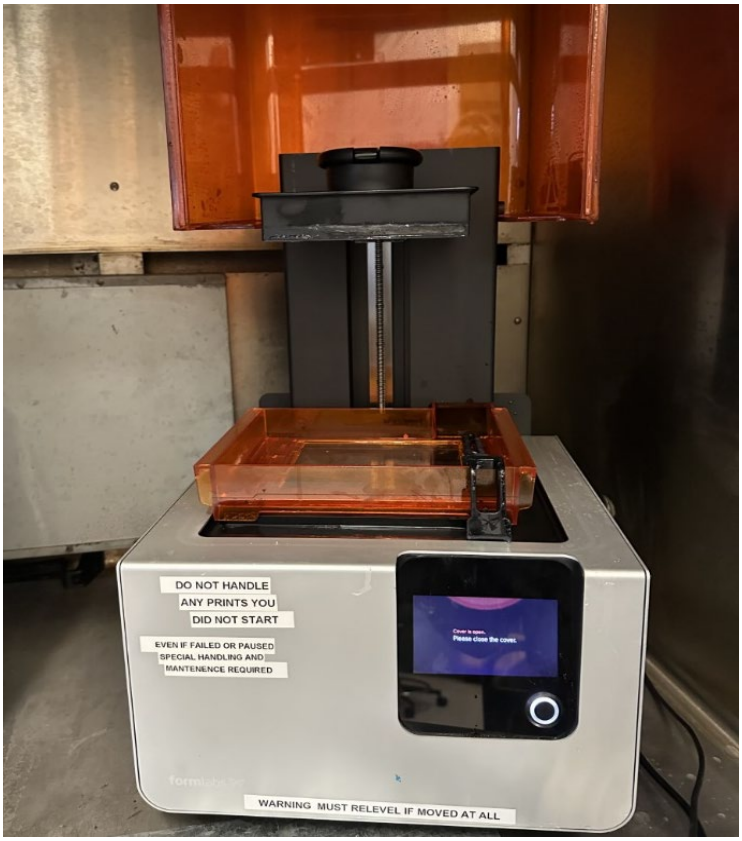

Figure 4. The FormLab 3D printer setup

A simple thin square model, whose thicknesses varied and will be discussed in Chapter IV, was uploaded to PreForm (FormLabs slicing software), and the model was "sliced" or sectioned into layers. This slicing process instructs the printer how to print each layer in terms of thickness and displays the model in the order that it would be printed. As will be discussed in Chapter IV, some issues with the printing of some of these samples led to the removal of support structures and even printing without the build plate.

C. FABRICATION OF COMPOSITES BY MOLD-CASTING

The first step in the molding fabrication was to dissolve as much PVDF in 100 mL of DMSO as possible without precipitation. Based on the previous fabrication method with the dissolve times of PVDF, it was decided that 6 grams of the PVDF would be the first amount to fully dissolve in 100 mL of DMSO. This process was done exactly as in the previous section: heating the DMSO to around 80°C in a beaker that is placed on a hot plate, inputting the desired amount of PVDF, and using a magnetic spinner to mix the solution until the powder fully dissolved.

One main difference in the casting done in this study compared to the mixing of resin for printing was that the BNNTs were added into the mixture after the PVDF was entirely dissolved. Adding BNNTs discolored the mixture making it difficult to examine if there was any solid PVDF remaining in the beaker. Another difference, the PR, which makes printing via STL possible, was not added to these mixtures to be cast.

Once mixing was completed, the mixture was poured into one of two different silicone molds shown in Figure 5. The filled molds were placed onto the hot plate and the temperature was elevated to speed the evaporation of the DMSO. The magnetic mixer was not used at this stage to prevent bubbling of the solution. Also, the temperature was not raised to the point of boiling the DMSO for the same reason: to prevent bubbling of the mixture.

Figure 5. The two molds that were used in the molding fabrication process

D. CHARACTERIZATION

1. Sample Metallization

Once a sample was either printed or cast, that sample was prepared for piezoelectric characterization. Both the top and bottom surfaces were coated with a conductive metal film, which served as the electrodes in the characterization of piezoelectric properties. One of two methods were used: painting with a quick-drying silver (Ag) paint or sputter coating the surfaces with a thin layer of Pt/Pd.

For sputter coating, the sides of the selected samples were painted with nail polish to keep the sides from being coated with Pt/Pd. The specimen was then placed onto the base plate of the sputter coater (208HR sputter coater, Cressington). Power to the control panel and the MTM-20 Thickness Monitor (Cressington) was turned on, energizing the vacuum pump. The argon (Ar) gas tank valve was opened allowing Ar gas to flood into the chamber. The samples to be coated were rotated through the coating process. The sample chamber was flushed with Ar. This involved opening the chamber to Ar and then pumping the chamber. This process was repeated three times until the chamber pressure dropped to 0.1 mbar. Ar then leaked into the chamber and a plasma was struck. Once a plasma plume was confirmed, a shield separating the sample from the plasma was removed and coating of the sample allowed for 30 seconds. After the sputtering took place, the shield was reinserted and the sputter coater was turned off, returning the sample to atmospheric

pressure. Pt/Pd coating thickness were on the order of 3–5 nm depending on the surface roughness of the samples. The sputter coater setup is shown in Figure 6.

The argon gas tanks and their pressure gauges are shown on the left of the crystal chamber with the connecting tube. The MTM-20 Thickness Controller is to the right of the chamber that the sample sits in, and they are both on top of the sputter coater machine.

Figure 6. The sputter coater

Once the sample was coated, acetone was used to remove the nail polish. The acetone removed not only the polish but the metal mist on top of it as well. The entire piezoelectric square did get sputter coated, but after the sputter coating was finished and acetone was used to remove the nail polish, the piece was left with bare sides, which was desired.

For samples that had Ag as the electrodes, the sides of the samples were first painted with nail polish just like samples that were sputter coated. Then the fast-drying Ag paint (Ted Pella) was applied to the top and bottom surfaces and allowed to dry. Once dry, acetone was used to remove the fingernail polish.

2. Contact Poling

Piezoelectric energy harvesters require orientation of the dipoles before energy harvesting can occur. For ceramics, the dipoles form because of a charge separation in the

unit cell of the ceramic crystal structure. For polymers, the dipole arises due to charge separation across individual monomers. In both cases, poling of the material is required. Typically, this is done by contact poling where a large electric field is applied across a sample arranged as a parallel plate capacitor (electrodes on the surfaces of the material) to induce movement of charged species to one electrode or the other.

A custom-made poling chamber was made from a desiccant chamber. Holes were drilled into the chamber to allow for wires that carry electrical current to and from a high voltage (HV) power supply (PolyK Products). To ensure safe operation of the poling station, the doors were fitted with a magnetic sensor. The sensor turns off power to the HV supply if the door is open. A Pyrex Tupperware is filled with silicone oil. Placed in the silicone oil is a test fixture designed for sample poling and ferroelectric testing, as shown in Figure 7. A red wire with its alligator clip is clamped to the top rod with a spring that is set above the sample and black wire is connected to the bottom plate where the sample rests. The silicone bath and test fixture with a sample is placed on top of a hot plate. Additional holes were drilled into the chamber for a power cable for the hot plate and a thermometer's thermocouple to monitor the temperature of the silicone oil bath. A schematic of the entire station is presented in Figure 8.

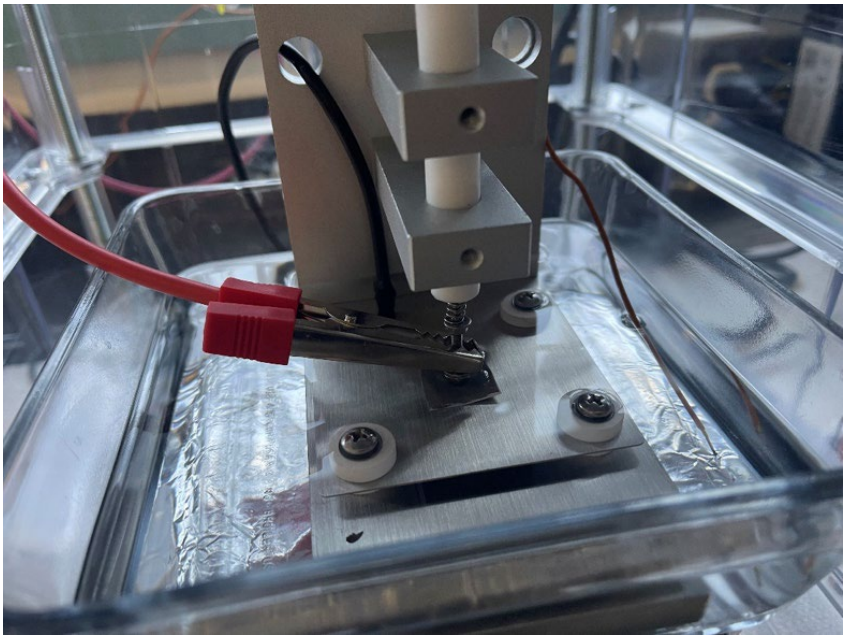

Figure 7. Silicone oil bath with piezoelectric test fixture

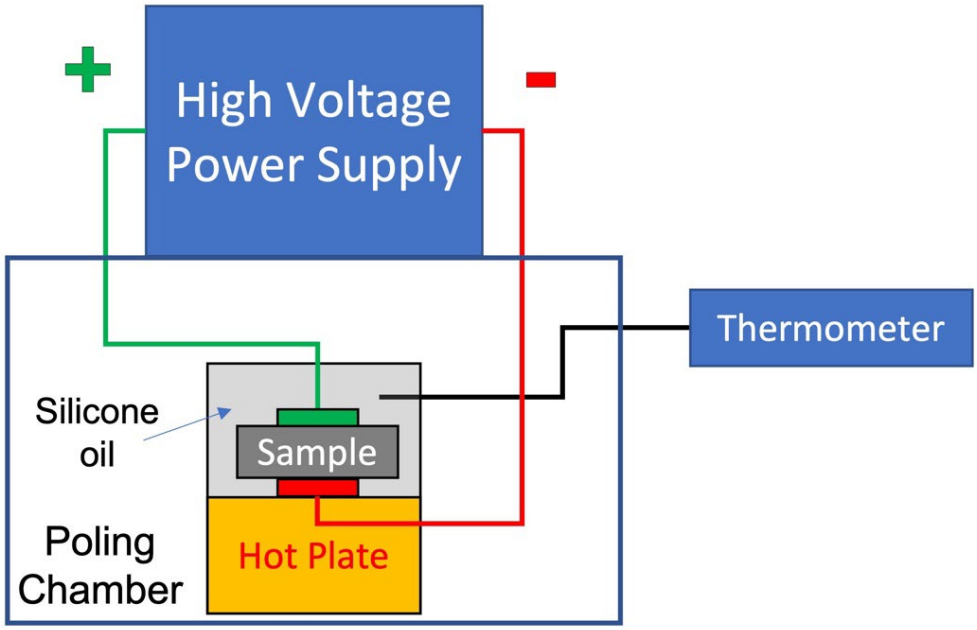

Figure 8. Schematic diagram of the contact poling station

The sample in the silicone oil bath is heated to an elevated temperature no higher than 80 °C. Once the targeted temperature is reached, voltage is applied to the sample through the HV supply. Voltage is slowly increased from 0 V up to 5 kV. The voltage applied depends on the electric field (in kV/mm or kV/cm), which itself depends on the thickness of the sample. The HV power supply has a built-in ammeter, which is used to monitor the current while voltage is increased. To avoid short circuiting of the sample, voltage increases are stopped when there is a sudden change in current or if the current surpasses 2 mA. Once the targeted voltage is reached, the voltage and temperature are maintained for 30–60 minutes, after which the voltage is returned to 0 V and the hot plate turned off and sample removed from the silicone oil bath.

3. Piezoelectric Characterization

For piezoelectric testing, a quasi-static Berlincourt piezoelectric d_{33} meter (PolyK Products) with a static force meter (PolyK Products) was used, as shown in Figure 9. The measuring process for the d_{33} piezoelectric charge constant was conducted by first zeroing the knob on the force sensor just enough so that the vibrations it projects could not be heard. The specimen being tested could then be inserted into the force sensor's clamp and the

knob tightened slightly. This tightening stabilizes the sample so that it does not move with the continuous vibrations but is not so tight that the sample surface is damaged.

Figure 9. Testing devices (shown counterclockwise from bottom): PolyK Berlincourt piezoelectric d_{33} meter, static force meter, and sample holder

IV. RESULTS

A. 3D- PRINTED SAMPLES

1. Mixture Components

Four different energy-harvester mixtures without BNNTs were printed and tested for an increase in piezoelectricity. After each print was tested, the ratios of mixture components were adjusted in hopes of achieving piezoelectric action out of the elements, which are discussed later in this chapter. Tables 1–4 summarize the data on each of the mixture components for the first, second, third, and fourth prints.

Table 1 shows the first attempt at creating an optimal piezoelectric element. For the remainder of this thesis, the table columns with green headers show the main comparison topic or difference within the table, the blue headers provide collected data, and the orange headers highlight the most important results; however, some tables will not have all three colors. The main takeaway from the first print attempt was that 10 grams of PVDF was too much for 100 mL of DMSO to dissolve, as about 1.5 grams of the solid had to be removed after more than an hour and a half of mixing. Additionally, the prints from this mixture were too brittle to test, so this mixture was not recreated and never got to the sputtering and polishing phases of the research.

Table 1. Summary of mixture components for the first set of prints

Component of mixture	Density	Inputted Amount	Dissolved Spin Rate (RPM)	Dissolve Time (Minutes)	Amount of PVDF removed [g]
DMSO	1.1 g/mL	100 mL	N/A	N/A	N/A
PVDF	1.77–1.82 g/cm^3	10 g	200	95	1.46
Clear PR	1.15–1.20 g/cm^3	100 mL	600	N/A	N/A

The density was determined from safety data sheets of each component of the mixture.

Table 2 summarizes the second mixture, where the biggest change was decreasing the amount of PVDF powder to 5 grams. Less PVDF had to be removed from this mixture and the dissolve time was shorter than the solution processed for the first print due to halving the amount of powder (10 grams to 5 grams) and increasing the spin rate of the magnetic mixer. This amount of PVDF (5 grams) was therefore carried forward for the next two prints as well. The amount of PR was also changed, increasing to 150 mL, because printing pieces from only 100 mL of resin was found to be slightly challenging due to having an insufficient amount of mixture.

Table 2. Summary of mixture components for the second set of prints

Component of mixture	Inputted Amount	Dissolved Spin Rate (RPM)	Dissolve Time (Minutes)	Amount of PVDF removed [g]
DMSO	100 mL	N/A	N/A	N/A
PVDF	5 g	400	65	0.716
Clear PR	150 mL	600	N/A	N/A

Table 3 summarizes the third print. The main difference between prints two and three was another increase in PR. This increase was an attempt to print more elements out of the 3D printer without changing the composition of the powder in the cartridge. The increase in PR allowed for more prints and easier handling of the mixtures. The piezoelectricity of each piece, however, did not increase when the PVDF solution was diluted. To improve piezoelectric properties, the PVDF was dissolved for a longer time to ensure complete dissolution of the powders.

Table 3. Summary of mixture components for the third set of prints

Component of mixture	Inputted Amount	Dissolved Spin Rate (RPM)	Dissolve Time (Minutes)	Amount of PVDF removed [g]
DMSO	100 mL	N/A	N/A	N/A
PVDF	5 g	400	150	0
Clear PR	200 mL	600	N/A	N/A

Table 4 summarizes the fourth print. Despite the challenges of having less PR in the mixtures, the amount of resin was decreased yet again to 100 mL. The amount of PR was decreased to increase the weight percent (wt%) of the PVDF powder in the overall mixture and, in turn, increase the piezoelectric active volume within the 3D printed sample. The Table 4 prints were the last mixtures tested without BNNTs. The Table 4 prints were significant because they were the first pieces that were printed with a reused resin tank. The reuse of resin tanks will be discussed later.

Table 4. Summary of mixture components for the fourth prints

Component of mixture	Inputted Amount	Dissolved Spin Rate (RPM)	Dissolve Time (Minutes)	Amount of PVDF removed [g]
DMSO	100 mL	Varies (base component)	N/A	N/A
PVDF	5 g	400	71	0.359
Clear PR	100 mL	600	N/A	N/A

2. 3D-Printing and Post-Processing

There were both successful and unsuccessful prints, categorized by their ability to be post-processed and tested. Some of the samples had slight variations in their printing processes and washing methods. The energy-harvesting prints were modeled in PreForm, a 3D printing software, at different thicknesses; however, the printer did not print them to their modeled depth. Each print was measured with calipers, and it was found that almost all the pieces printed were significantly thinner than their corresponding model. The modeled and actual thicknesses will be summarized after Table 5 is presented; however, the inaccuracy and unpredictability of the print's thicknesses is especially important to note. The thickness of the pieces will be referred to throughout this thesis by their modeled thicknesses because it is simpler to reference the thickness category the pieces are in, methodologically speaking, regardless of their actual thicknesses. The dimensions of the samples were chosen based on what was believed to be an optimal size for the piezoelectric energy-harvesters that would attach to the UAV. Thin prints were desired because narrower

pieces would allow the samples to be poled at lower electric fields. Conversely, larger samples with bigger surface area would provide more charge to the battery. The sturdiness of the prints was also prioritized in the selection consideration. For example, the 0.1 mm thickness prints would have been the optimal size for poling; however, they were extremely delicate to both print and handle, so they were ruled against for further testing. Additionally, the 30x30 mm prints would provide more charge than the 20x20 mm prints due to their larger surface area. However, the 20x20 mm prints did not curl after the isopropyl alcohol (IPA) wash like the larger 30x30 mm squares did, making post-processing easier. For these reasons, the 20x20x1 mm print, sample (e), was chosen to do future sputter coating and poling testing within the beginning stages of this research.

It is also important to note here that the third and fourth prints are not included in Table 5. These will be discussed in the sputter coating section because they are the two prints that were surface coated. Table 5 is solely to look at the modeling and printing of different mixtures that provided information on how to mix, print, and post-process other prints for the rest of the research. Additionally, because the prints from the fourth mixture reused its mixture's resin tanks, as briefly discussed previously, that mixture will have a separate table and discussion.

Table 5 also provides individual pictures for each of the parts, which can be mostly analyzed for opaqueness of the pieces in relation to their thickness as well as the curling or damage from post-processing.

Table 5. 3D printing and post-processing of the first two mixtures' prints

Width x Height [mm]	Modeled thickness [mm]	Actual thickness [mm]	PVDF powder [grams]	DMSO [mL]	PR [mL]	Build plate used	Build plate fully heated	Supports	Washing process	Photos of part
30 x 30	1	0.19	5	100	150	Yes	Yes	No	20 min on build plate	 Sample (a)
	0.5	0.08	5	100	150	Yes	Yes	No	20 min on build plate	 Sample (b)
	0.5	0.45	5	100	150	No	No	No	Free wash, ~20 min	 Sample (c)
	0.1	N/A	5	100	150	Yes	Yes	No	Free wash, ~20 min	 Sample (d)
20 x 20	1	0.23	5	100	150	Yes	Yes	No	20 min on build plate	 Sample (e)

Width x Height [mm]	Modeled thickness [mm]	Actual thickness [mm]	PVDF powder [grams]	DMSO [mL]	PR [mL]	Build plate used	Build plate fully heated	Supports	Washing process	Photos of part
	0.5	0.10	5	100	150	Yes	Yes	No	20 min on build plate	 Sample (f)
	0.1	0.51	5	100	150	No	Yes	No	Free wash, ~10 min	 Sample (g)
DNF	N/A	N/A	5	100	150	Yes	Yes	Yes	20 min on build plate	 Sample (h)
	N/A	N/A	10	100	100	Yes	Yes	Yes	20 min on build plate	 Sample (i)

The "build plate" column in Table 5 indicates whether a build plate was used for printing the part. The use of a build plate may seem standard since build plates are always used for FormLab prints. However, the 0.1 mm thick pieces were almost impossible to take off the build plate without damage, as seen with the 30x30x0.1 mm print, sample (d). Since scraping a 0.1 mm piece off a build plate could not be done without demolishing the part, printing this piece with no build plate was attempted.

Printing without a build plate was successful in this one instance because the samples were programmed to print with a 0.1 mm thickness in Preform. The layer thickness of the prints can be adjusted in Preform: the smaller the layer thickness, the more precise the piece. The increased precision of the pieces comes at the price of increased printing time; however, because these prints are so small, the time cost is insignificant. Since these parts were printed with 0.1 mm thickness layers, the printer formed only one layer for the 0.1 mm thickness pieces. The fact that the printer had to produce only one layer of hardened resin meant that the piece could be printed while freely floating within the PR because there was not a second layer to be added on top of it. If the print had needed another layer, as with the thicker prints, then the build plate would have been necessary to hold the first layer in place. Because the piece was left in the PR during printing, the sample was easily removed and set in the IPA wash machine. An example was sample (g), which was the thinnest of all samples printed or otherwise.

This printing process for the 0.1 mm thickness pieces seemed successful until the IPA wash. In Table 5, the pieces that were not formed on a build plate are labeled as "free wash" in the "washing process" column. These two data points correlate because free wash means that the printed pieces were submerged in the IPA without being attached to a build plate, which is dangerous to the piece because the wash creates a small whirlpool in the machine, and a freely floating print is likely to be damaged. The IPA machine is made for a build plate to be inserted into it prior to the piece being scraped off the build plate. The easily inserted build plate secures the print in the washing machine to produce a stable cleaning. When the pieces were post-processed with a free wash, the IPA did not harden them correctly. Therefore, sample (g) was printed with no build plate but did not dry correctly; it was sticky for weeks after it was washed. The stickiness was because the IPA

did not have as thorough and complete of a wash as it would have had the part been attached to a build plate; likely because the part was circulating in the IPA with little force exerted on its surface by the wash. But again, a 0.1 mm piece printed onto the build plate could not be taken off without damage. Therefore, it was decided that the 0.1 mm thickness parts were not feasible for printing, and that a build plate was necessary for the prints.

After printing of the 0.1 mm thickness pieces without a build plate, 0.5 mm thick prints were attempted with and without a build plate. Pieces with dimensions of 30x30x0.5 mm, labeled samples (b) and (c), were printed. The part with a build plate printed successfully; however, the part with no build plate did not. It was initially thought that the printer could produce the 0.5 mm parts as it did with the 0.1 mm pieces. However, since the layer thickness of the pieces was set to 0.1 mm in Preform, the 0.5 mm pieces needed five layers directly on top of one another in the PR with no build plate. Printing layers on top of one another that were freely floating in the PR was impossible without the anchoring that the build plate provided. The STL printing process printed two layers correctly on top of each other, but without the build plate holding them securely, the piece floated off in the PR and was no longer under the STL laser. Since the part still had three more layers to print, the 3D printer kept going; however, the other prints in the PR were unusable. The first square, which was free washed, was salvaged, and is shown in Table 5. However, similar to the 0.1 mm print, the part was sticky and unusable for testing.

The 0.5 mm pieces produced on the build plate printed in one piece and were not easily broken once removed from the build plate. However, these pieces were not chosen over the 1 mm thickness parts because the sides of the square samples curled significantly during the post-processing phase. Flattening them required placing a paperweight on top of them after the IPA wash, but this step highly increased the probability of their breaking off pieces or sticking to the paperweight if they were not fully dried. Additionally, once the pieces were mostly flattened and dried, their surfaces were brittle. The difficulty of handling the prints was a clear indication that they would be hard to test later, and therefore the 1 mm thickness parts were chosen.

Before completely disregarding the thinner prints, it is worth mentioning how the actual thicknesses of the pieces compared to their modeled thicknesses. Even though the

real and modeled thicknesses were never the same, there was a trend among how thick the printed pieces would be. For example, the 0.5 mm pieces always came out thinner than the 1 mm pieces, as expected. Additionally, the actual thicknesses of 1 mm and 0.5 mm pieces stayed around a similar value despite the composition of the print or its fabrication methods. The only trend that was unexpected was that the pieces that were printed without build plates always came out much closer to their modeled thickness than the pieces that were built on the build plate. In one case without a build plate, sample (g), the 0.1 mm piece printed thicker than its modeled thickness. The inaccuracy of the prints' thicknesses was never figured out.

Since 0.1 mm and 0.5 mm prints were excluded, the 1 mm thickness part as the chosen thickness for the prints. These parts were the only ones that could be post-processed and further handled without danger of breaking. It was decided that the 20x20x1 mm would be used over the 30x30x1 mm. The 30x30x1 mm would have been a good choice as well; however, for the initial testing, sturdiness was prioritized, and the 20x20x1 mm was harder to break and had no distortions in it after the IPA wash.

The "did not finish" rows in Table 5, denoted as DNF, include the parts that did not successfully print. These failed because of "supports," or additional PR that was printed solely to be discarded during the post-processing phase. These supports use more resin but allow the print to be optimally located on the build plate. Since the supports typically break off from the desired piece after it is fully printed and washed. Preform has the ability to generate optimal supports to securely print pieces, usually pieces with complex shapes. Printing the optimal supports was attempted for the first two prints; however, the printer stopped printing during the supports phase and did not generate the piezoelectric square element that was needed. The reason for the printer not completing the supports is thought to be because of the percentage of PVDF in the PR. Since the weight of the resin was heavier compared to its additives, it was harder for the mixture to create a part with any significant size. The printer's inability to produce the fully supported piezoelectric square elements is ultimately why the other prints were oriented to lay directly flat on the build plate, even though they could be more easily damaged in this orientation when scraping them off.

The temperature of the build plate was also taken into consideration. Sometimes the prints were started before the build plate was fully heated, shown by the "build plate fully heated" column. Whether the build plate was correctly warmed up or not was noted because a printer produces better parts when the PR in the resin tank is heated to certain temperatures. To determine whether there was a trend related to the temperature of the build plate, it was noted whether the pieces were printed on fully heated surfaces. When the system was not fully heated, it was not found to have any real effects on the pieces.

3. Fabrication with Reused Resin Tanks

Resin tanks had to be reused beginning on the fourth print. The resin tank is the portion of the 3D printer where the PR mixture lies while being hardened during the STL process, as shown in Figure 4. Reusing the orange resin tanks shown in Figure 4 was significant because resin tanks are fairly sensitive. A thin film at the bottom of the tank, where the prints are produced, is not supposed to be in contact with anything except the 3D printer and the resin that pours into it. Hands can touch the sides of the resin tank when inserting it into the printer, but nothing should touch the portion of the tank where the printing takes place because fingerprints can obstruct the optical path of the laser. Nevertheless, the resin tanks had to be reused because the FormLab 3D printers only accept certain tanks for certain resins. For example, a clear PR resin cartridge is not compatible with any other resin tank, so its liquid cannot pour into a tank made for a different resin: a chip in the bottom of each resin tank prevents them from being interchanged. Although this is a useful feature, when mixing and printing resin mixtures with slightly different ratios of components, such as in this research, equipment gets used up quickly.

Once the PR is poured into the resin tank from the cartridge, that tank is contaminated with that mixture, which cannot be fully removed due to the high viscosity of the PR. Tanks can typically be reused for up to 3,000 layers of printing with a given resin type; however, the tanks in this research could not be reused because, as previously stated, the mixtures changed frequently. Although the main component of the PR mixture was the compatible clear PR, this thesis tested different mixtures of PVDF/DMSO

individually; therefore, the cartridge had to be emptied and the resin tanks replaced to accurately test the performance of each print.

The supply of resin tanks was depleted after the first three prints; therefore, the fourth print was not only a test of a different mixture but also of whether the reuse of resin tanks was feasible for this project. To test whether they were reusable, the tanks were removed from the printer, and all of the PR that could be poured out of the tank was removed. IPA was then poured into the tank, covering the entirety of the bottom where the leftover resin lay. The IPA was left in the resin tank for about 24 hours. In reaction to the IPA, the leftover resin that could not be poured out of the resin tank hardened into a ductile sheet of hardened PR. This sheet could be removed from the resin tank without using mechanical means, such as scraping the sheets off, or otherwise touching the bottom of the tanks.

Once the resin tank was cleaned out with IPA, it was ready to be tested with a new mixture of PR/PVDF/DMSO. The reused tank was tested with the fourth print, the mixture summarized in Table 4. The fourth set of prints came out so well that they were the most used samples in the remainder of this work. Although the superior prints most likely came from the fourth mixture simply having a better ratio of PR/PVDF/DMSO, a major component of the print's fabrication method, the reuse of resin tanks, changed from the first three prints. The reusing of the resin tanks made no adverse difference in the prints; however, for the remainder of the research. Table 6 shows the printing and post-processing of the third and fourth prints. Table 6 shows the same information as Table 5, but with different mixtures and an acknowledgment that half of the prints reused a resin tank.

Table 6. Printing and post-processing of the third and fourth mixtures' prints

Width x Height [mm]	Modeled thickness [mm]	Actual thickness [mm]	PVDF powder [grams]	DMSO [mL]	PR [mL]	Build plate used	Build plate fully heated	Supports	Washing process	Photos of part
30 x 30	1	0.83	5	100	100	Yes	Yes	No	20 min on build plate	 Sample (j)
	1	0.78	5	100	200	Yes	Yes	No	20 min on build plate	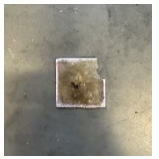 Sample (k)
20 x 20	1	0.67	5	100	100	Yes	Yes	No	20 min on build plate	 Sample (l)
	0.5	0.22	5	100	200	Yes	Yes	No	20 min on build plate	 Sample (m)

Table 6 shows that the same general trends from the first and second prints manifested in the third and fourth prints in terms of how they were fabricated and post-processed. One unexpected trend, however, is that the prints that utilized a reused resin tank, samples (j) and (l), had printed thicknesses much closer to their modeled thicknesses than previous samples. Recall that Table 5 had prints far less than half of their modeled thicknesses; however, three of the four prints in Table 6 are well over half of their modeled thicknesses. Samples (k) and (m) did not reuse a resin tank, so the successful modeling cannot be attributed to that variable alone; however, it should be reemphasized that the reuse of the resin tanks did not negatively affect the prints.

4. 3D Printing with BNNTs

Fabrication of the PVDF resin with BNNTs was the same as the fabrication of resin without BNNTs. The BNNTs came in a powder form like the PVDF and were added into the heated DMSO at the same time as the PVDF powder. Again, the powder components were mixed thoroughly with a magnetic mixer until they were fully dissolved. The solvent was heated to about 80°C, then the powders were added, as in the previous fabrication process. A summary of the mixtures with the BNNT print is shown in Table 7.

Table 7. Summary of mixture components for the one BNNT print

Component of mixture	Density	Inputted Amount	Weight Percent (wt%)	Dissolved Spin Rate (RPM)	Dissolve Time (Minutes)	Amount of powder removed [g]
DMSO	1.1 g/mL	100 mL	N/A	N/A	N/A	N/A
PVDF	1.77-1.82 g/ cm^3	4.748 g	94.97	600	62	0
BNNTs	2.29 g/cm^3	0.252 g	5..03	600	62	0
Clear PR	1.15-1.20 g/ cm^3	100 mL	N/A	600	N/A	N/A

The density was determined from safety data sheets of each component of the mixture.

The most significant difference between the composite and pure PVDF-TrFE powders is that the precursor powders were precisely measured rather than approximately with the whole numbers of 5 or 10 grams. The exact powder measurements were determined via an Excel sheet calculator. The spreadsheet calculated the mass of each powder based on the desired mass of total powder and a desired volume percent of 96% PVDF and 4% BNNTs, which produced the weight percentages in Table 7. For example, for the mixture described in Table 7, five grams was the value entered into the Excel calculator for the total mass of powder, and the corresponding weight for each powder was calculated based on that total value and the desired volume percentages for each powder: 4.748 grams and 0.252 grams of PVDF and BNNTs, respectively. The reason for the volume percentages of 96% PVDF and 4% BNNTs was to start with a small amount of BNNTs to test whether they could be used in fabrication without agglomerating, too much. BNNT agglomeration could lead to clogging of the printer nozzle.

An example of the Excel sheet calculator is in the Appendix, which shows a screenshot of the spreadsheet with the Table 7 mixtures' inputs and their corresponding results. To utilize the calculator, the user enters the required information into the three bolded cells: the chosen total mass of powder and the desired volume fractions of PVDF and BNNTs. The most significant equation within the Excel sheet is the one that calculates the weight fractions of either one of the powders, WF, based on the densities of the powders, ρ, and the desired volume fractions, VF. This equation is expressed as

$$\mathrm{WF}_1 = \frac{\rho_1 \mathrm{VF}_1}{\rho_1 \mathrm{VF}_1 + \rho_2 \mathrm{VF}_2}, \tag{2}$$

where the 1 and 2 subscripts denote either the PVDF data or the BNNT data, based on whichever weight fraction is being solved for. WF and VF are both percentages, while the ρ units, grams per cubic centimeter, cancel out. Equation (2) can be used to solve for the weight fraction of both powders; however, it can also be used to solve for just one of the weight fractions, and that answer can be subtracted from a value of one to obtain the weight fraction of the other powder.

Upon obtaining the weight fractions for both PVDF and BNNTs, those percentages were both multiplied by the total mass of powder to acquire the necessary amounts of each

powder that would be entered into the mixture. These are the values provided for the two powders under the "Inputted Amount" column in Table 7. The calculator was used for most of the future mixtures as well.

A factor that differed when mixing the BNNT powder into the solution was that the mixture took on the light gray color of the BNNT powder. This discoloration did not happen with the white PVDF, which dissolved fully in previous mixtures and left no tint in the DMSO solution. The murkiness of the mixture with BNNTs made it difficult to tell if any powder clumps still needed to dissolve in the solvent; however, once the mixture was taken off the heat and the resin was added and mixed again, the components were all thoroughly mixed and no solid material needed to be removed, as with some of the previous mixtures.

Other changes included the powders getting mixed into the DMSO at 600 RPM for the entire time they were dissolving to achieve faster dispersing times. The 3D printing fabrication method with BNNTs unfortunately did not get tested. The cartridge on the FormLab printer did not allow the mixture to pass into the resin tank. Although this fabrication approach was not successful, the mixing of BNNTs into PVDF helped to establish the best methods of fabrication in the next approach, the molding fabrication approach, which also incorporated BNNTs.

5. Electrical Characterization without BNNTs

The samples in Table 8 were chosen for poling as these prints came out the most manageable in terms of post-processing. For example, the four pieces that were poled were easily removed from the build plate and dried well after their IPA wash. They also kept their shape without curling or breaking. The amount of inputted PVDF within the piece was also considered with respect to the poling stages, which is why the amounts are shown again in Table 8. The weight percent of PVDF was important to analyze because the general trend should be that an increase in PVDF content within the piece provides an increase in the d_{33} reading.

Table 8. Summary of poling tests for samples without BNNTs

Method of metal coating	Sample	Amount of PVDF [g]	Time of poling [mins]	Silicon oil temperature [°C]	Applied voltage [kV]	Pre-poling d_{33} reading	Post-poling d_{33} reading
Sputter coating	(m)	5	30	66.7	1.5	0.03	0.03
	(k)	5	60	85.8	1.5	0.02	0.02
Silver Paint	(l)	5	60/30	63.4/76.8	2.0/6.0	0.02	0.2/0.2
	(j)	5	N/A	91	N/A	0.02	N/A

The main point of comparison within Table 8, however, is the method of metal coating applications to the samples. Both sputter coating and the manual application of silver (Ag) paint were tested during characterization to see if one method allowed for a larger increase in d_{33}. Although other poling methods were also tested, such as the time spent poling, the temperature of the silicon oil, and the applied voltage, the application of the metal coating was most important because it was a method of fabrication that was thought to have a large effect on the results of the poling tests.

The initial tested samples, (m) and (k), came from the same PR mixture, as shown in previous tables, but had different dimensions. Additionally, their method of metal coating was both sputtering. Because their poling results did not change, the poling methods were altered to try to increase the d_{33} reading. The amount of time that samples were poled for, along with the temperature of the silicon oil that the sample was poled within, was increased for the test on sample (j). An increased time and warmer environment are both ways to increase a d_{33} reading; however, it did not work for the sputter coated samples.

Because the d_{33} values remained the same for the sputter coated samples, some changes were made to this fabrication process in one last attempt to increase the d_{33} reading on the prints without BNNTs in them. The first change was the method of applying the metal coating. The Ag paint consisted of another noble metal and had the same purpose as the sputter coating process; however, the painting of the liquid metal was performed manually with a brush over the sample. This method was used rather than the lengthier, yet more controlled application of metal with sputter coating. Although the Ag paint

application would not be as precise as the Pt/Pd application within the sputter coating machine, any attempt to increase the d_{33} measurements was attempted at this point in the research. These changes in the metal coating process, both the application of the coating itself and the type of metal applied, did not provide an increase in the piezoelectric properties of the samples they were tested on.

Another changed testing parameter was the time spent poling, applied voltage, and temperature. All of these factors were increased on the third test if the sample would not change its d_{33} value with the initial applied voltages and an hour of poling, which it did not. This is why sample (l) in Table 13 has two values in several of its columns. The first numbers are the initial values tested on the piece, and the second values are the additional time, new temperature, and increased applied voltage, since the d_{33} reading was the same for the sample both before and after testing with its initial testing parameters. For example, sample (l) was tested for 60 minutes at 2 kV; however, its d_{33} reading was the same as before it was poled. Therefore, the same piece was tested again for an additional 30 minutes at 6 kV and a sharp 15°C temperature increase. 6 kV was chosen as the highest voltage to test because it was thought to be the highest value that could be applied without ruining the sample. The increase in the testing parameters failed, as shown by the same two values in the post-poling column; therefore, sample (j) was tested from the very beginning with the highest parameters.

Sample (j) was also unsuccessfully poled, but for different reasons. As previously discussed, heating the sample at too high of a temperature can cause damage to the element, which was unfortunately the case for sample (j). The silicon oil that had the sample in it was heated to about 91°C before the voltage was applied; however, it was evident there was a short-circuit within the sample because a large current went through the system when a voltage was applied. The short-circuit was attempted to be fixed by trimming the sides of the sample, but that did not work, so the piece could not be used for testing. Sample (j) remains in Table 13 as a reminder of the sensitivity of the pieces.

Also, the temperature readings on the thermometer from Figure 7 were not steadied to the exact temperatures in Table 13 for the entire test. The temperature values differed because the burn plate was very sensitive and did not read the temperature itself; rather,

the thermometer had to be inserted into the silicon oil that the sample was in while the knob on the plate was adjusted from 1 to 10. Once it was realized how finicky the burn plate was, the highest tested temperature value and the lowest were averaged and put into Table 13 for all of the samples.

Overall, Table 13 shows that for all of the samples that were sputtered and poled, none of their d_{33} readings increased, as was the goal for them. All of the tested samples became extremely brittle after their contact poling tests, especially the sputter coated samples. Due to not having an increase in the d_{33} measurements, the PVDF/DMSO/PR samples were discarded for the remainder of the research. The 3D printing and the PVDF/BNNT/DMSO samples were tested for the remainder of the project.

B. MOLDED SAMPLES

Because the 3D printing approach did not improve the piezoelectricity of the samples without BNNTs and did not allow for the incorporation of BNNTs, another fabrication method, mold casting, was explored. This approach used different molds of varying material to hold new mixtures of DMSO/PVDF/BNNTs and evaporate the solvent from the molds, leaving a film of PVDF/BNNTs for testing.

The first step in molding was to dissolve as much PVDF in 100 mL of DMSO without having to remove clumps of solid material. Based on the previous fabrication method's dissolve times relative to amounts of PVDF, it was decided that 6 grams of PVDF would be the first amount to fully dissolve in the DMSO. This process was done exactly as in the previous section: heating the DMSO to around 80°C in a beaker that is placed on a hot plate, inputting the desired amount of PVDF, and using a magnetic spinner to mix the solution until the powder fully dissolved. Another difference between these solutions and the printing resins was that the BNNTs were added into the mixture after the PVDF was entirely dissolved. The reasoning behind adding the two powders separately was because when BNNTs were added into the mixture for the last fabrication method, it discolored the entire solution and made it difficult to examine if there was any solid PVDF remaining in the beaker.

1. Mixture Components

Three mixtures were tested using the molding method. A summary of the mixtures and dissolving times for the first attempt of the molding fabrication method is shown in Table 9. The spin rate and dissolve times for each powder was also shown. Recall that the dissolve times were for each component separately since they were added one at a time until fully dissolved in hopes of a more thorough mixture. Therefore, the total mixing time is the combined PVDF and BNNTs dissolve times: 382 minutes in the case of the mixture from Table 9. The BNNTs were not expected to dissolve as the PVDF powder did, but rather to disperse evenly throughout the solvent. Still, the BNNTs had to be mixed into the solution to ensure that there was no agglomerated material in the solvent. Therefore, the BNNTs were mixed for an arbitrary time of 2.5 hours for the first mixture. It should also be noted that no resin was included in this mixture because the molding fabrication process did not use PR, only the 3D printing method did.

Table 9. Summary of mixture components for the first molded films

Component of mixture	Inputted Amount	Weight Percent (wt%)	Dissolved Spin Rate (RPM)	Dissolve Time (Minutes)
DMSO	100 mL	N/A	N/A	N/A
PVDF	6 g	94.97	600	232
BNNTs	0.318 g	5.03	600	150

Once the mixture was created, the magnetic mixer was removed from the beaker and the tinfoil that was used to help the beaker's contents retain their heat was discarded. The DMSO was then partially evaporated from the mixture while the solution was still in the beaker, before being poured into the molds. This involved boiling away some of the DMSO inside the beaker because the molds were not large enough to hold the amount of solution originally fabricated. Then the mixture was poured into a mold and the rest of the DMSO was allowed to evaporate.

a. Temperature Analysis

The boiling and melting points of each component of the mixture, as well as of the containers and molds had to be determined before evaporating the solvent to avoid contaminating the mixtures and/or damaging the molds and equipment. These temperatures are listed in Table 10. Once evaporation was complete, the left-over films found at the bottom of the mold or beaker were the solid samples that would be tested. A slightly higher DMSO boiling temperature compared to the powder's melting temperature was acceptable since the powders were supposed to form into a different shape when poured into the mold.

Table 10. Melting and boiling points for each material

Material	Melting point [°C]	Boiling point [°C]
DMSO	N/A	189 [28]
PVDF-TrFE	168 [29]	N/A
BNNTs	2000 [17]	N/A
Silicone Rubber	150	N/A

DMSO does not have a melting point listed because it is a liquid. The components that do not have boiling points listed are because they are solids. The sources are listed next to the respective boiling and melting point values for each of the temperatures. Silicone Rubber's melting point for the molds was received from a worker at the company via email.

The total amount of mixture within the beaker before the solvent was evaporated was noted to be about 110 mL for the first mold attempt. This value was important because it was necessary to boil away about half of the DMSO before pouring the solution into the mold. Therefore, an amount of solution of about 55 mL was desired before pouring the into any mold. The time for half of the solution to be boiled away was about 200 minutes. This time included the hot plate heating to the temperature that made the solution vaporize.

Because the mixtures were in a mold, there was not a full heat transfer from the hot plate to the solution. This was especially observable when evaporating the solvent. As the DMSO boiled away in the beaker during the intermediate step, the hot plate was increased to around 230°C rather than the 189°C boiling point from Table 10 to compensate for the

lack of full heat transfer from hot plate to solution, as well as to help offset the tin foil being removed and no longer retaining the heat of the mixtures. The thermometer helped to analyze what hot plate temperature kept the solution at the desired evaporation temperature. Even at a hotplate temperature of 230°C, the solution read about 160°C; not close to the necessary 189°C. However, the DMSO still turned to vapor, likely because closer to the hotplate, the temperature was hotter than where the thermometer was reading. Therefore, a hot plate temperature of about 230°C was ultimately chosen for boiling away the DMSO but was always validated with a thermometer. The inconsistent mixture temperatures were an issue throughout this research; however, this discussion explains how the problem was contended with. For the remainder of the research, the adjustment of the temperatures was accomplished in a similar way to correctly create the samples.

b. Punctured Mold

Once approximately 55 mL of solution remained, it was poured into silicone molds. Unfortunately, for the first mold attempt, there was a puncture in the bottom of the silicone mold because it was a hand-made mold with a 60 mm diameter, so some of the solution seeped onto the hot plate. The mold's bottom was then entirely removed, and the solution was allowed to lie directly on the plate. Although this mistake was not desired, it was clear that a film could still be created with the solution directly on the hotplate, so the rest of the solvent was left to evaporate. The first film did not have any definitive shape because of the mishap with the silicone mold, as the sides somewhat held the circular shape but not well; therefore, a rectangle was cut out of it, trying to retain as much of the film as possible. The rectangular film ended up being about 0.53 mm thick.

Once the film was obtained and its dimensions were cut to optimize the surface area, sputtering and contact poling was conducted. The sputtering was completed as previously discussed except without the nail polish process. Rather than painting the sides of the film to avoid a short circuit, clear Scotch tape was used to secure the sides of the sample to the bottom plate in the sputter coating machine, as shown in Figure 10. The resulting coated sample had electrodes like those seen in Figure 11.

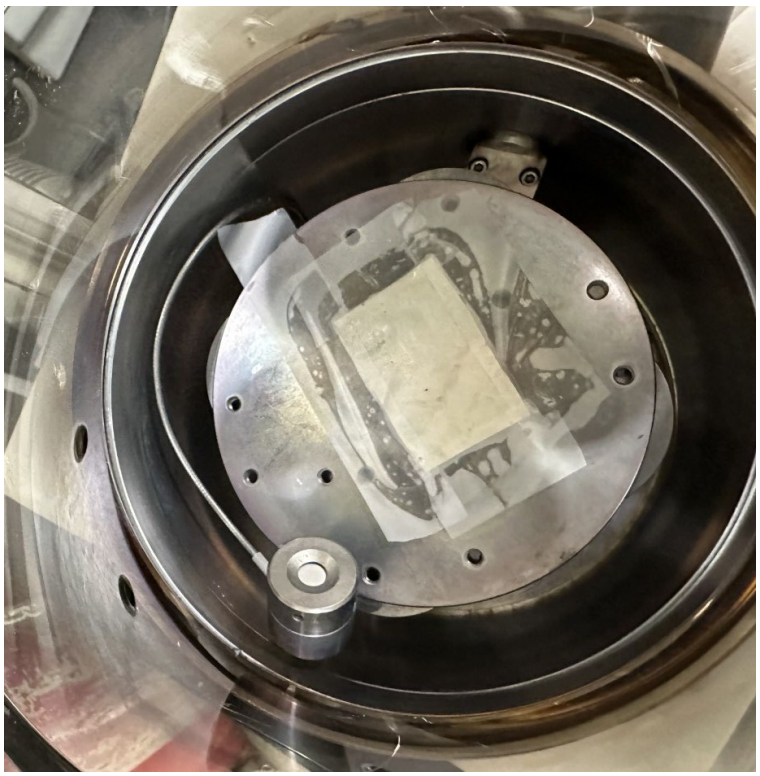

Figure 10. An example of the sample taped to the bottom plate in the sputter coating machine

Figure 11. The sample after the sputter coating process was conducted with Scotch tape.

For poling, the first molded sample was measured to have an average 0.3 mm thickness. So, an electric field of 5.0 kV/mm was desired for poling. Therefore, using Equation (1), a voltage of 1.5 kV was applied to the sample. The hot plate temperature was increased so that the silicon oil averaged 33.5°C. These values were found to not increase the d_{33} reading.

It should be noted that the first film that was fabricated from the molding process was an anomaly due to the punctured mold. The sample turned out to be much thinner than the molded films that were fabricated in molds that did not break. Although the first film's creation was not ideal, this sample did not have the surface irregularities that some of the unbroken molds exhibited. When boiling away the remainder of the solvent in unbroken molds, many air bubbles formed. Additionally, the next set of molds utilized had much higher sides than the initial mold that broke, making it difficult to create a uniform thickness throughout.

c. Unpunctured Molds

Table 11 shows the summary of the mixtures for the second and third films created through the molding method. Although there is only one table for this mixture, two samples came from this solution, as two different circular silicone molds (see Figure 5) were utilized in the fabrication process beyond this point: there was usually enough solution for more than one mold with each mixture, so more films could be created. The molds' exact dimensions do not matter since the samples were cut into squares during post-processing; however, the fact that they are circular molds will come into play later in this chapter when calculating expected thicknesses of the films was completed. Their diameters, however, were significantly different: 50.8 mm and 32.2 mm. The 50.8 mm diameter mold will be referred to as the "larger" silicone mold and the 32.2 mm diameter mold will be called the "smaller" mold. Table 11 summarizes these films' mixing components and fabrication information.

Table 11. Summary of mixture components for the second and third molded films

Component of mixture	Inputted Amount	Weight Percent (wt%)	Dissolved Spin Rate (RPM)	Dissolve Time (Minutes)
DMSO	100 mL	N/A	N/A	N/A
PVDF	9.372 g	93.72	800	162
BNNTs	0.628 g	6.28	800	120

Table 11 shows a few differences in the components for the second and third films relative to the first, including the amounts based on 10 grams of total powder and a desired 5 volume percent BNNTs. The increase of BNNTs was an attempt to increase the piezoelectricity within the samples. Due to the increased total amount of powder and volume percent of BNNTs, the weight percentages of BNNTs increased for this mixture, as shown when comparing Tables 9 and 11. Table 11 also shows that the spin rate increased relative to the first film mixture as well, while the dissolve times decreased. Unlike with the first film where it was removed, as the DMSO was later vaporized, the magnetic mixer was allowed to continue rotating at 600 RPM. The spinner was kept rotating because in the first film's fabrication, some of the powder hardened to the bottom of the beaker due to the high temperatures. Therefore, the mixer was allowed to continue to disperse the solid material for smoother construction of the film.

d. Post-Processing and Surface Irregularities

Of the two films, the film within the larger mold produced was a sturdy film that needed minimum post-processing. Post-processing in the case of molding included cutting the film into the largest square element possible, sanding the sides, and attempting to remove imperfections on the surfaces through flattening, sanding, and stretching. Surface imperfections resulted within the molded samples because of the inexactness in their fabrication process. For example, boiling away the DMSO caused small bubbles within the film that could not be avoided due to vapor generation within the mixture. The surface of the second film is shown in Figure 12 to visualize the imperfections that came from evaporating the DMSO in the mold. The sample in Figure 12 shows the bubbles that formed

on the surface of the molded films, likely due to the high evaporation temperatures. The molded films also had a texture that felt oily on the surfaces. This oily texture was likely due to a bit of leftover DMSO within the film, which became an issue in sputter coating.

Figure 12. The surface imperfections of the second molded film

Another issue in the second and third films was that the molds had to be filled by pouring the mixtures into them directly from the beaker, which did not allow for a perfectly even film thickness. The entirety of the solution was poured into the molds rather than attempting a thin film because the exact amount of DMSO left to be dissolved was not known. Due to pouring the entire solution into both of the molds arbitrarily, the second and third samples were much thicker than the 3D prints and the previous film, where much of the solution had to be discarded due to the mold breaking. Therefore, the entire solution was poured into the two molds for this part of the testing, which produced sturdier, thicker films. Moreover, although an attempt was made to smooth the surface of the solution with

a small powder spatula, it was difficult, especially compared to the smooth surface of the 3D printed films. Therefore, the thicknesses of the second and third films were an average approximation of several thickness measurements taken from each sample. The average thickness for these samples was 2.2 mm for the sample produced with the larger mold and 1.25 mm for the sample produced within the smaller mold. Figure 13 shows the cross-section of the third film, which highlights the imperfections of the thickness. Figure 13 also shows that the air bubbles formed throughout the mold and were a significant fraction of the overall film thickness. These bubbles were not ideal as the chances of a short-circuit occurring during poling increases, since a uniform voltage is applied depending on the overall average thickness of the sample. An air bubble would lead to thinner sections seeing that the same average voltage but now at higher electric fields potentially exceeding the threshold value, leading to an electrical shortage. This issue was combatted within the fourth film, which will be discussed later in this section.

Figure 13. A side view of the third molded film

The third film, which was the sample extracted from the smaller mold, needed more post-processing than the piece extracted from the larger mold because the side of the sample closest to the hotplate within the mold was severely burned. The burning of the smaller film likely resulted from the smaller dimensions of the mold itself. The heating process should have been conducted separately for the smaller and larger molds, with the hot plate temperatures being adjusted accordingly. However, due to having such a large amount of mixture, both molds were heated at the same time to evaporate the remainder of the solvent within them so that none of the solution would be contaminated and therefore unusable.

Sanding away the bubbles from the larger mold sample and the burnt parts of the smaller mold sample was attempted, but not completed successfully. The surfaces of the small samples were too hardened to significantly remove the imperfections by hand. Additionally, once the samples were cut into squares, air bubbles could be seen throughout most of the film, so eliminating them was impossible. Still, the samples were sputter coated and poled just as the first film was, which will also be described in the Characterization section.

Another film was tested from this solution as well. This film was not fabricated deliberately like the other three samples. This sample developed from the remainder of the powder in the beaker once most of the solution was poured into the molds. The beaker was left in the fume hood overnight, and a solid film from some of the left-over solution was extracted from the bottom of the beaker. The film was clearly not mixed well, as both fully white PVDF and fully gray BNNT portions of the film could be visually analyzed. However, the film averaged a thickness of 1.12 mm, much thinner than the deliberately fabricated films. Again, an optimized sized square piece was cut from the film for testing. The piece was sputtered and poled just as if it were fabricated on purpose. The sample immediately short-circuited within the silicon oil, so it will not be discussed in the next section; however, it was important to discuss that several different means of testing were conducted.

Table 12 summarizes the mixture components and dissolving information for the third solution of the molding fabrication method, which produced the fourth and fifth films.

This solution also used the two silicone molds and reverted to a mixture of 5 grams of total powder mass again to quicken the fabrication time.

Table 12. Summary of mixture components for the fourth molded film

Component of mixture	Inputted Amount	Weight Percent (wt%)	Dissolved Spin Rate (RPM)	Dissolve Time (Minutes)
DMSO	100 mL	N/A	N/A	N/A
PVDF	4.686 g	93.72	600	135
BNNTs	0.314 g	6.28	600	40

The fabrication process used in the previously molded films was mostly the same for the mixture summarized in Table 12. Again, the Excel spreadsheet was used to calculate the amounts of powders based on 95 volume percent PVDF and 5 volume percent BNNTs. The powders were mixed into the DMSO at the provided spin rates for the listed dissolve times. The solution was covered with tin foil and heated to about 80°C until the solution was thoroughly mixed. While evaporating the DMSO in the beaker, however, the magnetic spinner was left rotating so that no solid material formed at the bottom of the beaker and the powders did not harden without being in the mold.

What differed most importantly with this fabrication process was its more thorough evaporation of the solvent, as well as thickness. To ensure minimal air bubbles and avoid the results in Figures 12 and 13, the DMSO was evaporated at a much lower temperature than 230°C. Since there had been several anomalies with the temperatures throughout this research, 100°C was first tested for about four hours to see if any reduction in solvent volume would occur, but the volume appeared to remain unchanged. Therefore, the hotplate was increased to 200°C. This was slightly hotter than the 189°C solvent boiling temperature, so it would likely account for the hot plate heat transfer loss but was not so hot that it would burn the samples and trap vapor inside the solution.

In addition to the slower evaporation process, a thickness analysis was conducted. To avoid the uneven and unpredictable thicknesses of the films, calculations were

completed to help predict what the thicknesses of the samples from the molds should be if the materials were evenly distributed.

e. Thickness Analysis

As previously discussed, there was variability in the thicknesses of the second and third samples once they were removed from the molds, since it was difficult to evaporate the solvent from the mixture and still produce a film with even surfaces. Additionally, it was impossible to tell if all of the solvent had been boiled out of the film; even though solid samples were produced, only a visual inspection could be conducted. Additionally, the oily textures of most of the molds indicated that there was still solution left within them. To combat these issues, a more exact method was used to determine the expected thickness beginning with the fourth molded film.

To verify that the solvent was indeed fully evaporated out of the film, a thickness analysis was conducted to check that the sample in the mold was composed of only the powders. This thickness analysis was conducted by taking the density equation, which states that density is equal to mass divided by volume, and plugging in the terms for volume, V, where thickness is taken into consideration. This equation is expressed as

$$\rho = \frac{m}{V} = \frac{m}{0.25\pi d^2 t} \quad , \tag{3}$$

where ρ is the average density of the inputted powders in g/mm^3, m is the mass of total powder inputted into the mixture in grams, d is the diameter of the mold in millimeters, and t is the thickness of the film in millimeters. Equation (4) rearranges Equation (3) and solves for thickness.

$$t = \frac{4\,m}{\rho\pi d^2} \tag{4}$$

For this process, the average density of the BNNTs and PVDF was taken to be 0.00183 g/mm^3, the mass was the total amount of powder for that respective mixture, and the diameters depended on which mold was being used.

With these constant values known, the expected thicknesses of the fourth and fifth films could be solved for. However, the mass in Equation (4) is the total mass of the powder

if it were poured entirely into one mold. The solution was split between two molds. Therefore, the films were expected to be 1.34 mm and 3.36 mm with the entire solution poured into the larger and smaller molds, respectively. If these calculated values were about halved, those values would be approximately the average thickness of the samples when measured with a caliper. To avoid this variation, future molds could be weighed with and without the solution to see how much of the total mass was inputted into each mold.

In addition to the assumption that the entire solution was poured into one mold, the calculated thicknesses also did not take several fabrication obstacles into consideration. For example, the calculated values assumed smooth and even surfaces of the samples once they were removed from the molds and a constant thickness over the entirety of the film. Due to the pouring and evaporation processes, the surfaces were not smooth, and the measured thicknesses were always an average of several caliper measurements. To try to avoid surface imperfections, the DMSO was evaporated out of the mixture at lower temperatures. The slower evaporation process mitigated the large air bubbles that developed in the second and third films, as the fourth and fifth films had no noticeable surface imperfections.

To reduce surface imperfections even further, placing a weight onto one of the mixtures was attempted. Once the mixture was mostly solid within the larger mold, yet still somewhat fluid, a weight with a similar diameter to the larger mold was positioned on the top of the mixture. This mass weighed 30 grams and was used to smooth out the nonhomogeneous surface of the film. The weight sunk into the mixture more than hoped, as it was unable to sit at the surface and only push out the vapor bubble. It did ruin some of the mixture; therefore, the calculated thickness analysis was not expected to be accurate for the fourth film. However, an approximately 0.58 mm thick film was salvageable at the bottom of the weight. This film had no vapor bubbles and had a consistent thickness across the whole film. Therefore, it was concluded that the slower evaporation temperature helped with the air bubble issue, compared to films where no weight was added. To achieve both zero air bubbles and an overall even thickness within the sample, a weight was also necessary. The smaller film had inconsistencies in its overall thickness, however it was still sturdy and smooth, so it was sputtered and poled with the other sample.

After the thickness analysis was introduced for the fourth and fifth films, it was informative to do a similar analysis for the previous samples. The calculated thicknesses should scale with the mass of the powder introduced. For example, a ten-gram total powder input would ideally provide a thickness double that of a five-gram powder mixture. Knowing that the thickness calculations were scalable, and using Equation (4), the calculated thickness of each of the films could be found. Additionally, the thicknesses of the previous films could be compared to the amount of powder mixed into each solution to see if most of the solvent was evaporated out of the original films. Table 13 shows the calculated thickness and the average measured thickness of each film. Recall that the calculated thicknesses were halved due to the solution being split between two different molds, so the halved value and the average measured thicknesses should be compared.

Table 13. Melting and boiling points for each material

Film Number	Mold used	Total mass of powder [g]	Calculated thickness [mm]	Calculated thickness halved [mm]	Average measured thickness [mm]
1 *	Punctured mold (d = 60 mm)	6.318	1.22	0.61	0.35
2	Larger mold (d = 50.8 mm)	10	2.70	1.35	2.2
3	Smaller mold (d = 32.2 mm)	10	6.71	3.36	1.25
4 *	Larger mold (d = 50.8 mm)	5	1.34	0.67	0.58
5	Smaller mold (d = 32.2 mm)	5	3.36	1.68	0.97

An asterisk is placed next to the film number if the two values were not expected to be close due to issues in the fabrication, such as with the weighted sample and the punctured mold, where much of the mixture had to be discarded.

Table 13 shows inconsistencies in more than just the films for which a dissimilar calculated and averaged measured thickness were expected, even when the calculated thicknesses were halved, as none of the thicknesses came close to what was anticipated.

These inconsistencies were expected even before conducting the thicknesses analysis. Firstly, halving the calculated value was not accurate because the amount of solution poured into each mold was not measured; the solution was poured based on visual inspection, not by a weight or thickness. Additionally, the larger mold was not exactly double the size of the smaller mold. The halving calculation was just to get a more accurate thickness value, but there were still issues with exactness because it was still just a rough approximation.

The discrepancies in Table 13 could also be due to the wide array of thicknesses in each of the films, especially the second and third films, where numerous vapor bubbles littered the sample. Although about five measurements were taken for each sample, one at each corner and one in the center, this was still an extremely loose average. For example, in the fifth film, there was a portion about 0.2 mm thick and one about 1.6 mm thick. These two measurements were taken into account for the average since they were at opposite corners of the sample; however, the extremes of these measurements do not help when comparing to a calculated thickness with several assumptions, since they make the actual average thickness very different from the calculation.

If film thickness became a more significant factor in this research, there are several methods to make the measured thicknesses more comparable to the calculated thicknesses, such as weighing how much solution is poured into each mold, fine-tuning the addition of weights into the molds, and improved temperature trial-and-error testing.

However, the thickness analysis was conducted simply to get a more accurate guess if the solvent was entirely dissolved from the films. Although the thicknesses were not particularly comparable, it can still be assumed that most of the DMSO evaporated from the samples. This assumption can be made especially for the fourth and fifth films due to the slower evaporation process and the addition of a weight on the mixture. Not only did the fourth and fifth samples not have any vapor bubbles on their surfaces, they also did not have the oily texture that the first few samples did. The lack of moistness on the films showed that less solvent was retained in the last two film samples.

2. Sputtering and Poling for the Last Two Films

Once the thickness analysis was completed for the discarded films and the fourth and fifth films, the latter films were sputtered and poled. The same process was completed as previously. The only difference for sputtering was the sputtering time. Rather than 30 seconds, providing a 4 nm thickness of Pt/Pd, the sputter coater was run for 60 seconds, providing a metal coating of about 8 nm. A thicker metal coating was applied in hopes for a better poling process. The results will be discussed in the Characterization Section.

3. Electrical Characterization of Molded Films

Table 14 shows that none of the molds' the post-poling d_{33} measurement increased. As previously discussed, the second and third mold films were much thicker than any of the other samples due to pouring the entirety of the solution into the molds. Therefore, desiring an electric field of 5.0 kV/mm and inputting the thicknesses into Equation (1) would have meant using a higher voltage than the machine could produce. Therefore, the testing voltages started at 1.5 kV and increased in increments, if the sample allowed for it without short-circuiting.

Table 14. Summary of poling tests for molded films

Film Number	Weight % of PVDF	Thickness of sample [mm]	Time of poling [mins]	Silicon oil temperature [°C]	Applied voltage [kV]	Pre-poling d_{33} reading	Post-poling d_{33} reading
1	94.97	0.3	30	33.5	1.5	0.03	0.03
2	93.72	2.2	N/A	N/A	1.5	0.02	N/A
3	93.72	1.25	60	63.4	1.5/2	0.02	0.0/0.05
4	93.72	0.58	N/A	N/A	1.5	0.02	NA
5	93.72	0.97	60	22	3	0.02	0.02

The second film has several N/A sections due to the immediate short-circuiting of the sample. The short-circuit was likely due to surface imperfections. Therefore, the third film was tested. This film was the one that had the burnt side, so it was not expected to be

successful. However, this piece did not immediately short-circuit. It did have some current running through the piece, but the value of the current uncharacteristically decreased within the hour that the sample was poled. About 30 minutes into poling, the voltage was increased to 2 kV due to the decreased current, hence the two values in this portion of Table 14. As the voltage increased, so did the current, but again it decreased as poling went on.

After 60 minutes of poling for the third film, the sample was removed from the silicon oil and the d_{33} value was measured. Unusually, one side of the sample provided a d_{33} value of 0.00 and the other side provided a value of 0.05. Recalling previous discussion, both sides should read the same d_{33} value except with opposite signs. After further examination of the sample, it was clear the much of the sputter coated Pt/Pd had been washed away from the surfaces by the oil. The removal of this metal likely explained both the current phenomena and the different post-poling d_{33} value measurements.

As always with poling the samples, the temperature of the silicon oil and the time poled vary based on what the sample is expected to be able to handle. For example, the thinner first film was only poled for 30 minutes at about half of the temperature as the third film. Yet still, the voltage was not increased for the thicker samples immediately due to current flow. Many times, throughout the course of this research, each of these parameters had been pushed to higher temperatures, voltages, and poling times in an attempt to get an increased post-poling d_{33} value but the sample was ruined. Therefore, the values in the samples are constantly varied based on what is thought to be optimal for the sample rather than a calculation.

Like the second film, the fourth film had several N/A sections due to the immediate short-circuiting of the sample. After analyzing the sample, the short-circuit was likely due to part of the print being too thin, or slightly opaque in some sections. The fifth film was therefore tested in the last attempt of the research to get an increase in d_{33} measurements. The voltage was increased to 3 kV for this test because the sample was able to handle that voltage, as no current went through the sample at any point in the voltage increase. Unlike other tests, however, the silicon oil was left at room temperature, 22°C. The temperature was left at room temperature because that had not been tested before, and it was thought that several of the samples may have been ruined by the hot temperature of the silicon oil

due to the smell the system produced in some cases. However, despite the higher voltage and the steady temperature, the fifth sample did not increase its d_{33} value, remaining at a value of 0.02 both before and after poling.

THIS PAGE INTENTIONALLY LEFT BLANK

V. CONCLUSIONS AND FUTURE WORK

A. CONCLUSIONS

Stereolithography based fabrication of PVDF-TrFE-BNNT composites were investigated. For the printed samples, it is likely that the reason that changes to polarization was not demonstrated was due to the amount of PR that was in the samples. Much of the volume of the samples was not PVDF (i.e., piezoelectrically active) but rather the non-piezoelectric resin, which decreased the likelihood of creating a piezoelectric sample and possibly caused the unsuccessful poling results. Another reason for not seeing increasing d_{33} readings could have been due to the inhomogeneous distribution of powder within the prints. This was indicated by the non-uniform appearance of the samples when held to light where small darker patches could be seen within the samples. Although the 3D printer produced sturdy samples to measure the d_{33}, expected increases were not observed.

For the mold casting samples, the lack of an increase in the d_{33} measurements likely came from not achieving sufficiently high electric fields to polarize the sample, as these pieces were usually thicker than the 3D printed samples. Polarization of the monomers in PVDF-TrFE may have occurred but below the saturation polarization. So, samples saw changed orientation of the dipoles but did not retain polarization increases. Electrically elastic tendencies occur when the diploes revert back to their original orientation upon removal of the applied field. This behavior is seen in non-ferroelectric piezoelectric materials like α-quartz. In PVDF, however, remanent polarization should be observed but only if the poling procedure achieves sufficiently high electric fields. For the composites investigated in this work, saturation polarization was not achieved.

B. FUTURE WORK

In future work, if printing is attempted again, it might be better to use FFF. Although this printing approach was initially decided against because it was unknown whether printable filament could be extruded, FFF could be used to print uniform and sturdy polymer composites. FFF could likely produce more physically solid samples composed entirely of the PVDF and any composite fillers. FFF printed PVDF composites

may even serve as a structural component on the UAV, which would have better strength to uphold UAV applications. FFF would also likely distribute the powder more homogenously throughout the samples, as it uses filament and not liquid resin. It may even be possible to print an entire UAV with the PVDF composite.

Whether it was the restriction of the volume of piezoelectric activity with too much PR in the STL method or by the inability to create a large enough electric field for the mold casting approach, none of the samples demonstrated an increase in their d_{33} measurements. However, there was success in certain areas. Several of the samples did not immediately short circuit, which means that there was probably microscopic poling within the samples that could not be measured with the ex-situ d_{33} method that was used in this research. Therefore, more testing could take place to find a successful electric field value. Additionally, there are a plethora of potential modifications to the fabrication methods that could be made to improve performance of the samples, including attempting different ratios of piezoelectric powders within each mixture, or attempting different techniques of printing or casting. By finding different methods that lead to an increase in d_{33} measurements after poling, the samples could then be attached to a UAV to test the original objectives of the research.

APPENDIX. EXCEL SHEET CALCULATOR

Powder	Density	Units	Source				
PVDF-TrFE	**1.8**	g/cm^3	Piezotech SDS			VF =	Volumn Fraction
BNNT	**2.29**	g/cm^3	BN Nano			WF =	Weight Fraction
	Total Mass:		**5**	grams			
	PVDF and BNNT :						
	Desired VF BNNT		**4%**				
	Desired VF PVDF		**96%**				
	Calculated WF BNNT		5.03%				
	Calculated WF PVDF		94.97%				
		BNNT	0.252	grams			
		PVDF	4.748	grams	Needed for Mixture		

THIS PAGE INTENTIONALLY LEFT BLANK

LIST OF REFERENCES

[1] X. Xu, Y. Zeng, Y. L. Guan, and R. Zhang, "Overcoming Endurance Issue: UAV-Enabled Communications with Proactive Caching," *IEEE J. Sel. Areas Commun.*, vol. 36, no. 6, pp. 1231–1244, Jun. 2018, doi: 10.1109/JSAC.2018.2844979.

[2] S. A. H. Mohsan, M. A. Khan, F. Noor, I. Ullah, and M. H. Alsharif, "Towards the Unmanned Aerial Vehicles (UAVs): A Comprehensive Review," *Drones*, vol. 6, no. 6, p. 147, Jun. 2022, doi: 10.3390/drones6060147.

[3] W. Jaafar and H. Yanikomeroglu, "Dynamics of Laser-Charged UAVs: A Battery Perspective," *IEEE Internet Things J.*, vol. 8, no. 13, pp. 10573–10582, Jul. 2021, doi: 10.1109/JIOT.2020.3048087.

[4] P. J. Bártolo, Ed., *Stereolithography*. Boston, MA: Springer U.S., 2011. doi: 10.1007/978-0-387-92904-0.

[5] M. Marandi and J. Tarbutton, "Additive Manufacturing of Single- and Double-Layer Piezoelectric PVDF-TrFE Copolymer Sensors," *Procedia Manuf.*, vol. 34, pp. 666–671, 2019, doi: 10.1016/j.promfg.2019.06.194.

[6] C. Aumnate, A. Pongwisuthiruchte, P. Pattananuwat, and P. Potiyaraj, "Fabrication of ABS/Graphene Oxide Composite Filament for Fused Filament Fabrication (FFF) 3D Printing," *Adv. Mater. Sci. Eng.*, vol. 2018, pp. 1–9, Nov. 2018, doi: 10.1155/2018/2830437.

[7] H. Kim *et al.*, "3D Printing of Polyvinylidene Fluoride/Photopolymer Resin Blends for Piezoelectric Pressure Sensing Application Using the Stereolithography Technique," *MRS Commun.*, vol. 9, no. 3, pp. 1115–1123, Sep. 2019, doi: 10.1557/mrc.2019.109.

[8] N. Sezer and M. Koç, "A Comprehensive Review on the State-of-the-Art of Piezoelectric Energy Harvesting," *Nano Energy*, vol. 80, p. 105567, Feb. 2021, doi: 10.1016/j.nanoen.2020.105567.

[9] K.-A. N. Duerloo, M. T. Ong, and E. J. Reed, "Intrinsic Piezoelectricity in Two-Dimensional Materials," *J. Phys. Chem. Lett.*, vol. 3, no. 19, pp. 2871–2876, Oct. 2012, doi: 10.1021/jz3012436.

[10] J. E. Lee, R. Nam, M. B. Jakubinek, B. Ashrafi, and H. E. Naguib, "Development of PVDF Nanocomposite with Single-Walled Carbon Nanotubes (SWCNT) and Boron Nitride Nanotubes (BNNT) for Soft Morphing Actuator," *Smart Mater. Struct.*, vol. 30, no. 5, p. 055014, May 2021, doi: 10.1088/1361-665X/abf23d.

[11] H. Kawai, "The Piezoelectricity of Poly (vinylidene Fluoride)," *Jpn. J. Appl. Phys.*, vol. 8, no. 7, p. 975, Jul. 1969, doi: 10.1143/JJAP.8.975.

[12] L. Ruan, X. Yao, Y. Chang, L. Zhou, G. Qin, and X. Zhang, "Properties and Applications of the β Phase Poly (vinylidene fluoride)," *Polymers*, vol. 10, no. 3, p. 228, Feb. 2018, doi: 10.3390/polym10030228.

[13] C. K. McGinn *et al.*, "Formulation, Printing, and Poling Method for Piezoelectric Films Based on PVDF–TrFE," *J. Appl. Phys.*, vol. 128, no. 22, p. 225304, Dec. 2020, doi: 10.1063/5.0027855.

[14] R. I. Haque, R. Vié, M. Germainy, L. Valbin, P. Benaben, and X. Boddaert, "Inkjet Printing of High Molecular Weight PVDF-TrFE for Flexible Electronics," *Flex. Print. Electron.*, vol. 1, no. 1, p. 015001, Mar. 2016, doi: 10.1088/2058-8585/1/1/015001.

[15] N. Yanar, E. Yang, H. Park, M. Son, and H. Choi, "Boron Nitride Nanotube (BNNT) Membranes for Energy and Environmental Applications," *Membranes*, vol. 10, no. 12, p. 430, Dec. 2020, doi: 10.3390/membranes10120430.

[16] J. H. Kim, T. V. Pham, J. H. Hwang, C. S. Kim, and M. J. Kim, "Boron Nitride Nanotubes: Synthesis and Applications," *Nano Converg.*, vol. 5, no. 1, p. 17, Dec. 2018, doi: 10.1186/s40580-018-0149-y.

[17] J. H. Kang *et al.*, "Multifunctional Electroactive Nanocomposites Based on Piezoelectric Boron Nitride Nanotubes," *ACS Nano*, vol. 9, no. 12, pp. 11942–11950, Dec. 2015, doi: 10.1021/acsnano.5b04526.

[18] K. S. Kim *et al.*, "Polymer Nanocomposites from Free-Standing, Macroscopic Boron Nitride Nanotube Assemblies," *RSC Adv.*, p. 9, 2012.

[19] S. Laha, A. Chakraborty, and T. K. Maji, "Synergistic Role of Microwave and Perturbation toward Synthesis of Hierarchical Porous MOFs with Tunable Porosity," *Inorg. Chem.*, vol. 59, no. 6, pp. 3775–3782, Mar. 2020, doi: 10.1021/acs.inorgchem.9b03422.

[20] Y. Okumura, J. Koyama, H. Takaku, H. S, "Influence of Organic Solvents on the Growth of Marine Microalgae," *Arch. Environ. Contam. Toxicol.*, vol. 41, no. 2, pp. 123–128, Sep. 2001, doi: 10.1007/s002440010229.

[21] C. Vinodbabu, G. T. Rao, N. B. Reddy, and G. V. Zyryanov, "A Review on Magnetron Sputter Coatings," presented at the Proceedings of International Conference on Recent Trends in Mechanical and Materials Engineering: ICRTMME 2019, Chennai, India, 2020, p. 040052. doi: 10.1063/5.0018142.

[22] J. Sarkar, "Sputtering and Thin Film Deposition," in *Sputtering Materials for VLSI and Thin Film Devices*, Elsevier, 2014, pp. 93–170. doi: 10.1016/B978-0-8155-1593-7.00002-3.

[23] K. Nakamatsu, K. Kanda, Y. Haruyama, T. Ichihashi, T. Kaito, and S. Matsui, "Mechanical Property Evaluation of Au-coated Nanospring Fabricated by Combination of Focused-Ion-Beam Chemical Vapor Deposition and Sputter Coating," *J. Vac. Sci. Technol. B Microelectron. Nanometer Struct.*, vol. 24, no. 6, p. 3169, 2006, doi: 10.1116/1.2397068.

[24] C. Lee and J. A. Tarbutton, "Electric Poling-Assisted Additive Manufacturing Process for PVDF Polymer-Based Piezoelectric Device Applications," *Smart Mater. Struct.*, vol. 23, no. 9, p. 095044, Sep. 2014, doi: 10.1088/0964-1726/23/9/095044.

[25] E. R. Cholleti, "A Review on 3D Printing of Piezoelectric Materials," *IOP Conf. Ser. Mater. Sci. Eng.*, vol. 455, p. 012046, Dec. 2018, doi: 10.1088/1757-899X/455/1/012046.

[26] B. Jaffe, *Piezoelectric Ceramics*. Academic Press Inc., 1971.

[27] P. Curie, "Fundamentals of Piezoelectricity," 2021.

[28] National Center for Biotechnology Information, "PubChem Compound Summary for CID 679, Dimethyl Sulfoxide," [Online]. Available: https://pubchem.ncbi.nlm.nih.gov/compound/dimethylsulfoxide#section=Taste

[29] D. E. Septiyani Arifin and J. J. Ruan, "Study on the Curie Transition of P(VDF-TrFE) Copolymer," *IOP Conf. Ser. Mater. Sci. Eng.*, vol. 299, p. 012056, Jan. 2018, doi: 10.1088/1757-899X/299/1/012056.

THIS PAGE INTENTIONALLY LEFT BLANK

INITIAL DISTRIBUTION LIST

1. Defense Technical Information Center
   Fort Belvoir, Virginia

2. Dudley Knox Library
   Naval Postgraduate School
   Monterey, California